Evaluation of potential designs for a continuous epoxidation reactor

Gustavo V. Olivieri, Jacyr V. de Quadros Jr., Reinaldo Giudici*

Universidade de São Paulo, Escola Politécnica, Department of Chemical Engineering, Av. Prof. Luciano Gualberto, Travessa 3, No. 380, 05508-010, São Paulo, Brazil

Keywords: Epoxidation reaction; Epoxidized soybean oil; Simulation; Continuous reactor.

ABSTRACT - A continuous reactor for the epoxidation of soybean oil has been considered in various studies, with various designs. In practice, the existing commercial plants continue to use batch reactors, due to capital cost optimization and safety concerns. This article carries out a simulation of a continuous tubular reactor (based on a detailed kinetic model from our previous work), proposing a single addition of all reagents in the absence of catalysts and emulsifiers. The design combines the robust model developed on the basis of bench experiments with industrial experience to evaluate the viability of a continuous flow model. The study provides an analysis of the effects of static mixers in the reaction system, focusing on the safety of the reactor associated with the temperature profile, the quality parameters associated with the epoxidation of vegetable oils (iodine and oxirane indexes), as well as the acceptable pressure drop. Promising results were obtained from simulations of a proposed reactor design, in which an oxirane index of 5.95% (79.1% net yield of the desired product) was achieved for a 120 minute residence time under the most viable conditions.

1. Introduction

A current tendency in chemical industries is the use of substances extracted from biomass as raw materials to synthesize several products. In particular, vegetable oils may be used for the production of biodiesel, epoxidized products, alkyd resins, coatings, lubricants, etc. ^{1,2}

Epoxidized vegetable oils are substances derived from the epoxidation reaction of vegetable oils. These products can be applied as secondary plasticizers for polyvinyl chloride as an alternative to petroleum-derived phthalates. Epoxidized soybean oil (ESO), for example, has positive properties such as biodegradability, non-volatility, and low flammability, besides originating from a renewable source (soybean oil). These characteristics can be contrasted with the health implications associated with phthalates, justifying their replacement by ESO.²⁻⁴

The epoxidation of vegetable oils is usually based on the Prileschajew reaction, in which the vegetable oil reacts with an organic peracid. The organic peracid is usually generated *in situ* from the reaction of hydrogen peroxide with a carboxylic acid, employing a biphasic system to obtain the epoxidized product. The system also involves undesired reactions, such as the degradation of the oxirane ring of the epoxidized products and the decomposition of the peracid. A summary of the reaction system is presented in Figure 1. Moreover, adequate stirring is required for this two-phase liquid-liquid system in order to assure an adequate contact surface between the phases and enhance the mass and heat transfer. In a previous study, a comprehensive kinetic model was developed for this reaction system, including all of the mentioned chemical reactions, a description of the heat and mass transfer, and the effects of the apparent kinematic viscosity.

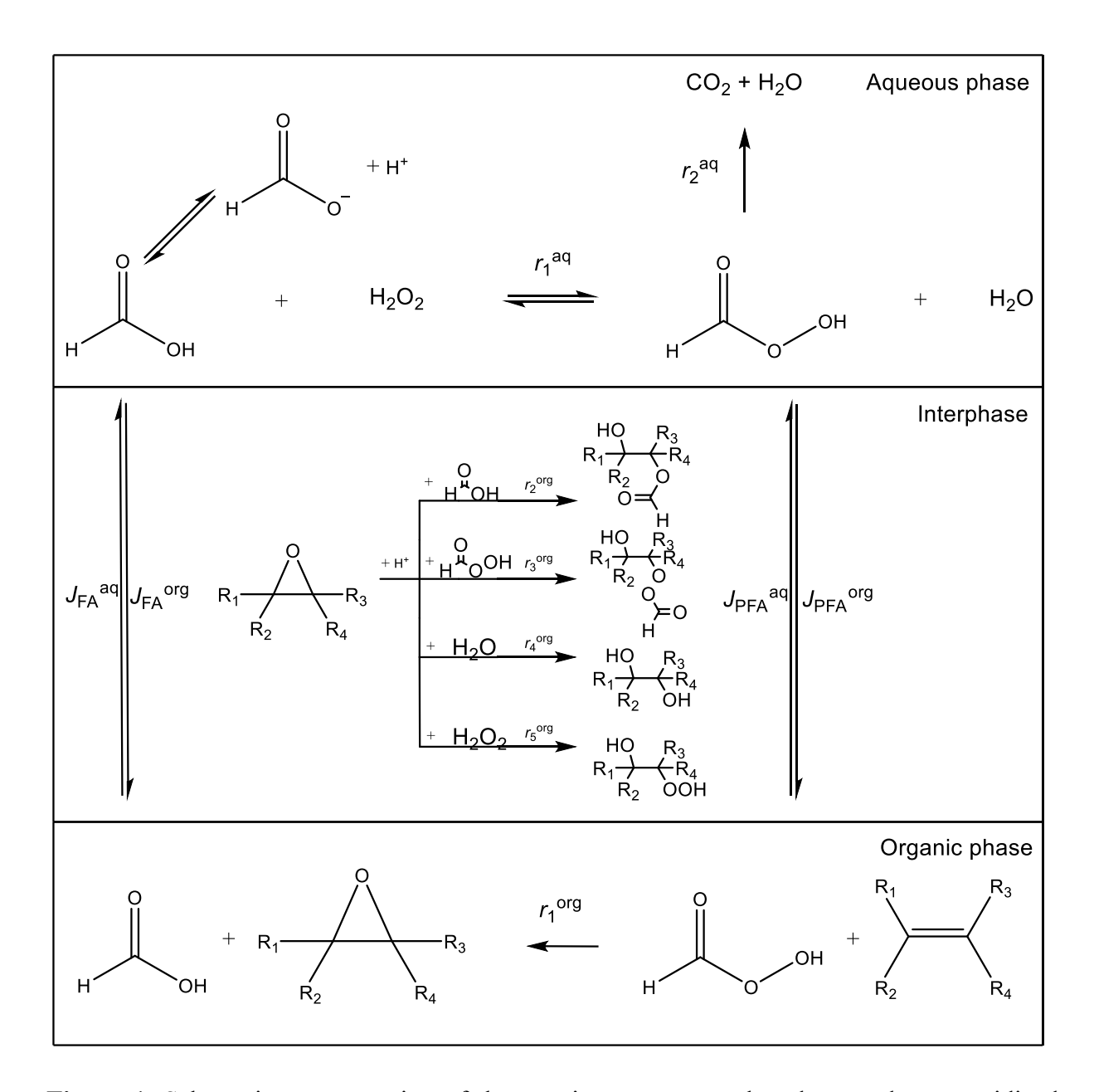


Figure 1. Schematic representation of the reaction system employed to produce epoxidized soybean oil (from ref. 11, with permission of ACS).

Traditionally, this reaction is conducted in a batch system due to capital cost optimization and safety concerns. Nevertheless, an increase in productivity can be expected when the process is performed in continuous reactors, especially tubular reactors. Some authors have analyzed this reaction using tubular reactors on micro- or milliscales (named micro- or millireactors). The results

were promising, reducing the reaction time considerably from the order of hours to the order of minutes. ^{12–18} Most of these studies involved the use of stabilizers and/or catalysts such as mineral acids, enzymes, or titanium- or tungsten-based catalysts. The exceptions were the work of Vanoye et al., ¹⁵ who studied the epoxidation reaction via a different synthetic route, the Mukaiyama reaction, and the simulation study of Cortese et al., ¹⁸ which analyzed the viability of operating the reactor at temperatures above the usual range for this system, i.e., surpassing 100 °C.

As a continuation of our previous studies of the epoxidation reaction of soybean oil, ^{11,19} the present work evaluates the viability of employing a continuous tubular reactor, based on the comprehensive reaction model ¹¹ and a proposed design based on industrial experience that includes real-life possibilities and safety measures. The simulations were performed considering a single addition of the main reactants, in the absence of catalysts or stabilizers, together with an analysis of the effects of static mixers in the reactor.

2. Methodology

2.1. Process conditions

The reactor feed consisted of 1000 kg·h⁻¹ of a pre-mixed two-phase system containing soybean oil as the organic phase and an aqueous phase containing hydrogen peroxide and formic acid. The flow rate of 1000 kg·h⁻¹ provides a projected capacity of approximately 7 kt/yr of epoxidized soybean oil, considering a conservative production schedule. This value was considered for these evaluations as it represents the capacity of a base unit of production for a Brazilian company that has been operating for more than 10 years in the segment. The proportions of the reactant phases, determined based on the batch reaction analysis presented in our previous study¹¹, were 68.5% organic phase and 31.5% aqueous phase, on a weight basis.

The feedstock that constituted the aqueous dispersed phase of the feed stream was 87 parts by weight of 85 wt% formic acid and 13 parts by weight of 60 wt% hydrogen peroxide. The feedstock for the continuous organic phase was pure soybean oil, with an iodine index of 129 g I₂/(100 g oil). The reactor's inlet stream was considered to be pre-heated to a temperature of 333.15 K and pre-mixed, with the aqueous phase dispersed as spherical droplets. No accumulation was considered in the interphase between the dispersed aqueous phase and the continuous aqueous phase.

The reactor consisted of a cylindrical stainless-steel tube, immersed in water at a constant temperature. Two different tube diameters were analyzed, with nominal diameters of just over 1 in (0.0266 m) and 2 in (0.0525 m). An average value of 2 h was assumed for the residence time of the reaction media inside the reactor. The axial dispersion was neglected in the studied cases, although radial dispersion was included in order to verify whether there is a significant radial variation in temperature that could influence the reaction performance.

The behavior of the reactors was analyzed under three different scenarios: (1) in the absence of static mixers; (2) in the presence of Raschig rings as static mixers inside the whole volume of the reactor; (3) in the presence of a determined number of Sulzer SMXTM static mixers locally distributed along the reactor. For scenario (1), the droplet size of the aqueous phase was estimated based on the shear from the fluid flow, while for scenarios (2) and (3), the droplet size was determined considering the shear due to the static mixers. For scenario (3), in which the static mixers do not fill the whole reactor, the droplet size was assumed to remain constant, i.e., droplet coalescence was neglected during the residence time between two consecutive static mixers. This assumption was derived from an experimental observation of coalescence of the biphasic system, in which the phases take several hours to become completely separated.

The Raschig rings were assumed to have an internal diameter of 3 mm and an external diameter and height of 4 mm, leading to a fixed bed with porosity estimated as 73%, an equivalent spherical particle diameter of 3.48 mm and sphericity of 0.384.

The Sulzer SMXTM static mixer consists of repeatedly sets of crossed bars inside a tube, providing changes in the flow direction and leading to an efficient mixing. Schemes of these static mixers can be found on the website of Sulzer.²⁰ The values related to the Sulzer SMXTM static mixer were collected from the study of Legrand et al.:²¹ porosity of 77%, tortuosity of 1.5, pore diameter of 0.75 mm, and length of 14.5 mm.

Table 1 summarizes the cases studied, in which D_t is the tube diameter, T_{ext} is the external water temperature, N_{SMX} is the number of Sulzer SMXTM static mixers, and L_t is the length of the tube. The L_t value was estimated based on the average value for the residence time (2 h), the cross-section area of the tube, the flow rate of the reaction media (1000 kg·h⁻¹ or 0.278 kg·s⁻¹) and the bed porosity.

Table 1. Specifications of the cases studied.

Case	Static mixer	$D_{\rm t}$ / m	$L_{\rm t}$ / m	$T_{\rm ext}$ / K	$N_{ m SMX}$
01	No	0.0266	3711	313.15	-
02	No	0.0266	3711	333.15	-
03	No	0.0525	953	313.15	-
04	No	0.0525	953	333.15	-
05	Raschig rings	0.0266	5084	313.15	-
06	Raschig rings	0.0266	5084	333.15	-
07	Raschig rings	0.0525	1306	313.15	-

08	Raschig rings	0.0525	1306	333.15	-
09	Sulzer SMX TM	0.0266	3711	313.15	4
10	Sulzer SMX TM	0.0266	3711	333.15	4
11	Sulzer SMX TM	0.0525	953	313.15	4
12	Sulzer SMX TM	0.0525	953	333.15	4
13	Sulzer SMX TM	0.0525	953	313.15	10
14	Sulzer SMX TM	0.0525	953	313.15	20
15	Sulzer SMX TM	0.0525	953	313.15	30
16	Sulzer SMX TM	0.0525	953	313.15	40
17	Sulzer SMX TM	0.0525	953	313.15	50

Additionally, it is important to detail the basis for the proposal of scenario (3). In this scenario, the reactor was divided into segments in series determined by the number of Sulzer SMXTM static mixers, with each segment containing a pumping station, the static mixer and part of the tube. Moreover, both extremities of the segments, associated with the pumps, were assumed to be open to the atmosphere. Figure 2 summarizes this arrangement corresponding to the tube segment dimension for scenario (3), jointly with schemes for scenarios (1) and (2).

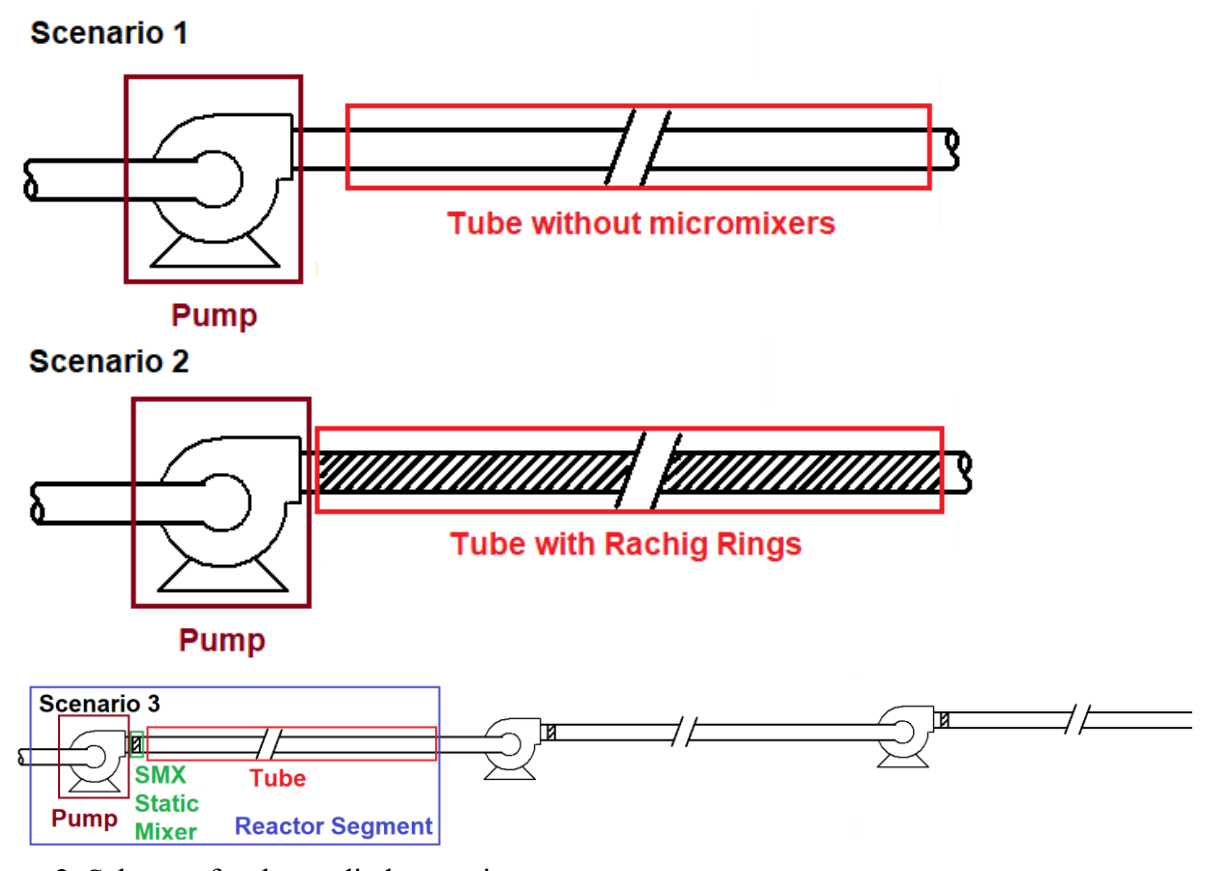


Figure 2. Schemes for the studied scenarios.

Evidently, several other scenarios could be analyzed as well. The three scenarios mentioned were chosen for the simulations for the sake of comparison, although some limitations may be expected in the first two scenarios: the absence of static mixers may compromise the mass transfer effects between the phases, while the use of static mixers, especially Raschig rings, tends to increase the pressure drop of the flowing reaction system. These points will be compared and extensively analyzed after presenting the results.

2.2. Computational support

The present simulation study was based on a model that is discussed in depth in the next section.

The model consists of a system of partial differential equations (PDEs) and includes several

algebraic equations. The system of equations was solved using a MATLAB (version R2015a) code, including the "pdepe" command.

2.3. Modeling

The simulation of the reaction system was performed considering both axial and radial variations of the properties in the tube and steady state operation. An axial symmetry was considered in the tube, which allowed the system to be described with a 2D geometry.

The continuity equation for species i in phase j was described as eq (1):²²

$$v_z \frac{\partial c_i^j}{\partial z} = \frac{d_i^j}{r} \frac{\partial}{\partial r} \left(r \frac{\partial c_i^j}{\partial r} \right) + R_i^j + J_i^j \tag{1}$$

where v_z is the velocity in the axial direction, c is the molar concentration, d is the kinetic rate, d is the mass transfer molar rate per unit of volume, d is the axial position, and d is the radial position. In this context, d may represent the mass diffusion coefficient d (scenarios (1) and (3)) or the radial mass dispersion coefficient d (scenario (2)).

The boundary conditions associated with this partial differential equation are described by eqs (2) to (4), in which the subscript 0 refers to the feed conditions and D_t is the pipe diameter.

$$c_i^j\big|_{z=0} = c_{i,0}^j \tag{2}$$

$$\left. \frac{\partial c_i^j}{\partial r} \right|_{r=0} = 0 \tag{3}$$

$$-d_i^j \frac{\partial c_i^j}{\partial r} \Big|_{r=D_1/2} = 0 \tag{4}$$

The application of eq 1 for the main substances of the reaction led to eqs (5) to (12).

$$v_{z} \frac{\partial c_{\text{FA}}^{\text{aq}}}{\partial z} = \frac{d_{\text{FA}}^{\text{aq}}}{r} \frac{\partial}{\partial r} \left(r \frac{\partial c_{\text{FA}}^{\text{aq}}}{\partial r} \right) - R_{1}^{\text{aq}} - R_{2}^{\text{org}} \left(\frac{\phi^{\text{org}}}{\phi^{\text{aq}}} \right) + J_{\text{FA}}^{\text{aq}}$$

$$(5)$$

$$v_{z} \frac{\partial c_{\text{HP}}^{\text{aq}}}{\partial z} = \frac{d_{\text{HP}}^{\text{aq}}}{r} \frac{\partial}{\partial r} \left(r \frac{\partial c_{\text{HP}}^{\text{aq}}}{\partial r} \right) - R_{1}^{\text{aq}} - R_{5}^{\text{org}} \left(\frac{\phi^{\text{org}}}{\phi^{\text{aq}}} \right)$$

$$\tag{6}$$

$$v_{z} \frac{\partial c_{\text{PFA}}^{\text{aq}}}{\partial z} = \frac{d_{\text{PFA}}^{\text{aq}}}{r} \frac{\partial}{\partial r} \left(r \frac{\partial c_{\text{PFA}}^{\text{aq}}}{\partial r} \right) + R_{1}^{\text{aq}} - R_{2}^{\text{aq}} - R_{3}^{\text{org}} \left(\frac{\phi^{\text{org}}}{\phi^{\text{aq}}} \right) + J_{\text{PFA}}^{\text{aq}}$$

$$(7)$$

$$v_z \frac{\partial c_{\rm W}^{\rm aq}}{\partial z} = \frac{d_{\rm W}^{\rm aq}}{r} \frac{\partial}{\partial r} \left(r \frac{\partial c_{\rm W}^{\rm aq}}{\partial r} \right) + R_1^{\rm aq} + R_2^{\rm aq} - R_4^{\rm org} \left(\frac{\phi^{\rm org}}{\phi^{\rm aq}} \right)$$
 (8)

$$v_z \frac{\partial c_{\text{PFA}}^{\text{org}}}{\partial z} = \frac{d_{\text{PFA}}^{\text{org}}}{r} \frac{\partial}{\partial r} \left(r \frac{\partial c_{\text{PFA}}^{\text{org}}}{\partial r} \right) - R_1^{\text{org}} + J_{\text{PFA}}^{\text{org}}$$
(9)

$$v_z \frac{\partial c_{\text{DB}}^{\text{org}}}{\partial z} = \frac{d_{\text{DB}}^{\text{org}}}{r} \frac{\partial}{\partial r} \left(r \frac{\partial c_{\text{DB}}^{\text{org}}}{\partial r} \right) - R_1^{\text{org}}$$
(10)

$$v_{z} \frac{\partial c_{\text{FA}}^{\text{org}}}{\partial z} = \frac{d_{\text{FA}}^{\text{org}}}{r} \frac{\partial}{\partial r} \left(r \frac{\partial c_{\text{FA}}^{\text{org}}}{\partial r} \right) + R_{1}^{\text{org}} + J_{\text{FA}}^{\text{org}} \tag{11}$$

$$v_z \frac{\partial c_{\text{EG}}^{\text{org}}}{\partial z} = \frac{d_{\text{EG}}^{\text{org}}}{r} \frac{\partial}{\partial r} \left(r \frac{\partial c_{\text{EG}}^{\text{org}}}{\partial r} \right) + R_1^{\text{org}} - R_2^{\text{org}} - R_3^{\text{org}} - R_4^{\text{org}} - R_5^{\text{org}}$$
(12)

in which ϕ is the volumetric fraction, the superscripts aq and org refer to the aqueous and organic phases, respectively, and the subscripts FA, PFA, HP, W, DB, and EG denote formic acid, performic acid, hydrogen peroxide, water, double bonds of the soybean oil, and epoxide groups of the epoxidized soybean oil, respectively.

The energy equation for the system can be described by eq(13):²²

$$\rho^{\text{ave}} C_p^{\text{ave}} v_z \frac{\partial T}{\partial z} = \frac{\lambda^{\text{ave}}}{r} \frac{\partial}{\partial r} \left(r \frac{\partial T}{\partial r} \right) - \sum_j \left[\left(\sum_q \Delta H_q^j R_q^j \right) \phi^j \right]$$
(13)

where T is the temperature, ρ is the density, C_p is the heat capacity on a mass basis, λ is the thermal conductivity, ΔH is the enthalpy of reaction, and the superscript ave denotes an average value between the phases.

The boundary conditions associated with the partial differential equation 11 are described by eqs (14) to (16).

$$T|_{z=0} = T_0 (14)$$

$$\left. \frac{\partial T}{\partial r} \right|_{r=0} = 0 \tag{15}$$

$$-\lambda^{\text{ave}} \frac{\partial T}{\partial r}\Big|_{r=D_{t}/2} = U_{\text{ext}} \left(T|_{r=D_{t}/2} - T_{\text{ext}} \right)$$
(16)

in which $T_{\rm ext}$ is the temperature of the heat transfer fluid and $U_{\rm ext}$ is the global heat transfer coefficient that includes the resistances to heat transfer through the reactor wall and that of the external side of the reactor tube.

The kinetic equations are summarized in Table 2, the mass transfer equations in Table 3 and the physical properties in Table 4, following the model proposed in our previous study.¹¹

Table 2. Summary of the kinetic equations of the model

Equation	Eq. number	Ref.
$R_1^{\text{aq}} = k_1^{\text{aq}} c_{\text{H}^+}^{\text{aq}} \left(c_{\text{HP}}^{\text{aq}} c_{\text{FA}}^{\text{aq}} - c_{\text{PFA}}^{\text{aq}} c_{\text{W}}^{\text{aq}} / K_1^{\text{aq}} \right)$	(17)	11
$R_2^{\rm aq} = k_2^{\rm aq} c_{\rm PFA}^{\rm aq}$	(18)	11
$R_1^{\text{org}} = k_1^{\text{org}} c_{\text{DB}}^{\text{org}} c_{\text{PFA}}^{\text{org}}$	(19)	11
$R_2^{\text{org}} = k_2^{\text{org}} a_{\text{V}} c_{\text{EG}}^{\text{org}} c_{\text{H}^+}^{\text{aq}} c_{\text{FA}}^{\text{aq}} (\phi^{\text{aq}} / \phi^{\text{org}})$	(20)	11
$R_3^{\text{org}} = k_3^{\text{org}} a_{\text{V}} c_{\text{EG}}^{\text{org}} c_{\text{H}^+}^{\text{aq}} c_{\text{PFA}}^{\text{aq}} (\phi^{\text{aq}} / \phi^{\text{org}})$	(21)	11
$R_4^{\mathrm{org}} = k_4^{\mathrm{org}} a_{\mathrm{V}} c_{\mathrm{EG}}^{\mathrm{org}} c_{\mathrm{H}^+}^{\mathrm{aq}} c_{\mathrm{W}}^{\mathrm{aq}} (\phi^{\mathrm{aq}}/\phi^{\mathrm{org}})$	(22)	11
$R_5^{\text{org}} = k_5^{\text{org}} a_{\text{V}} c_{\text{EG}}^{\text{org}} c_{\text{H}^+}^{\text{aq}} c_{\text{HP}}^{\text{aq}} (\phi^{\text{aq}} / \phi^{\text{org}})$	(23)	11
$k_q^j = k_{q,r}^j \exp[(E_q^j/R)(1/T_r - 1/T)]$	(24)	11
$K_1^{\text{aq}} = K_{1,r}^{\text{aq}} \exp[(\Delta H_1^{\text{aq}}/R)(1/T_r - 1/T)]$	(25)	11
$c_{ m H^+}^{ m aq} = \sqrt{c_{ m FA}^{ m aq} 10^{-pK_{ m a}}}$	(26)	11
$pK_{a} = -57.528 + 2773.9/T [K] + 9.1232 \ln T [K]$	(27)	23

Table 3. Summary of the mass transfer equations of the model.

Equation	Eq. number	Ref.

$$J_{i}^{\text{aq}} = \beta_{i}^{\text{aq}} a_{\text{V}} \left(c_{i}^{\text{org,eq}} H_{i} - c_{i}^{\text{aq}} \right)$$

$$J_{i}^{\text{org}} = \beta_{i}^{\text{org}} a_{\text{V}} \left(c_{i}^{\text{org,eq}} - c_{i}^{\text{org}} \right)$$

$$\beta^{\text{org}} = \beta^{\text{aq}} \phi^{\text{aq}} / \phi^{\text{org}}$$

$$(29) \qquad 24$$

$$\beta^{\text{org}} = \beta^{\text{aq}} \phi^{\text{aq}} / \phi^{\text{org}}$$

$$(30) \qquad 25$$

$$c_{i}^{\text{org,eq}} = \frac{\beta^{\text{aq}} c_{i}^{\text{aq}} \phi^{\text{aq}} + \beta^{\text{org}} c_{i}^{\text{org}} \phi^{\text{org}}}{\beta^{\text{aq}} H_{i} \phi^{\text{aq}} + \beta^{\text{org}} \phi^{\text{org}}} = \frac{c_{i}^{\text{aq}} + c_{i}^{\text{org}}}{H_{i} + 1}$$

$$(31) \qquad 11$$

$$H_{\text{FA}} = c_{\text{FA}}^{\text{aq,eq}} / c_{\text{FA}}^{\text{org,eq}} = \left[9 \cdot 10^{-7} (T [\text{K}])^{2} - 5.42 \cdot 10^{-4} T [\text{K}] + 0.0854 \right]^{-1}$$

$$(32) \qquad 25$$

$$H_{\text{PFA}} = c_{\text{PFA}}^{\text{aq,eq}} / c_{\text{PFA}}^{\text{org,eq}} = \left[4 \cdot 10^{-6} (T [\text{K}])^{2} - 2.23 \cdot 10^{-3} T [\text{K}] + 0.3496 \right]^{-1}$$

$$(33) \qquad 25$$

Table 4. Summary of the equations used to calculate the physical properties.

Equation	Eq. number	Ref.
$\rho^{\text{ave}} = 1/(w^{\text{aq}}/\rho^{\text{aq}} + w^{\text{org}}/\rho^{\text{org}})$	(34)	
$C_p^{\text{ave}} = w^{\text{aq}} C_p^{\text{aq}} + w^{\text{org}} C_p^{\text{org}}$	(35)	
$\lambda^{\text{ave}} = w^{\text{aq}} \lambda^{\text{aq}} + w^{\text{org}} \lambda^{\text{org}}$	(36)	
$\rho^{\text{aq}} \left[\text{kg·m}^{-3} \right] = 1508.2 - 0.9415 \ T [K]$	(37)	26,27
$\rho^{\text{org}} \left[\text{kg·m}^{-3} \right] = 1112.9 - 0.657 \ T \left[\text{K} \right]$	(38)	27
$C_p^{\text{aq}} \left[\mathbf{J} \cdot \mathbf{k} \mathbf{g}^{-1} \cdot \mathbf{K}^{-1} \right] = 3043.2 + 0.2594 \ T \left[\mathbf{K} \right]$	(39)	27,28
$C_p^{\text{org}} \left[J \cdot kg^{-1} \cdot K^{-1} \right] = 1020.1 + 2.9412 T [K]$	(40)	27
$\lambda^{\text{aq}} \left[\mathbf{W} \cdot \mathbf{m}^{-1} \cdot \mathbf{K}^{-1} \right] = -0.1010 + 3.694 \times 10^{-3} \ T \left[\mathbf{K} \right] - 4.254 \times 10^{-6} \ (T \left[\mathbf{K} \right])^{2}$	(41)	29
$\lambda^{\text{org}} \left[\mathbf{W} \cdot \mathbf{m}^{-1} \cdot \mathbf{K}^{-1} \right] = 0.9459 - 4.584 \times 10^{-3} \ T \left[\mathbf{K} \right] + 6.380 \times 10^{-6} \ (T \left[\mathbf{K} \right])^{2}$	(42)	30
$\mu^{\text{aq}} [\text{Pa·s}] = 1.8588 \times 10^{-4} \exp[54.640/(T[\text{K}] - 273.15)]$	(43)	31
$\mu^{\rm org} = \mu_{\rm DB} + (\mu_{\rm EG} - \mu_{\rm DB})X$	(44)	
$\mu_{\rm DB} [\text{Pa·s}] = 1.9099 \times 10^{-4} \exp[764.81/(T [\text{K}] - 162.74)]$	(45)	32

$$\mu_{\text{EG}} [\text{Pa·s}] = 2.4180 \times 10^{-4} \exp[1306.5/(T[\text{K}] - 117.33)]$$
 (46)

The mass diffusion coefficient for an i substance in the j phase ($d_{\text{diff},i}^{j}$) was estimated using the procedure detailed by Riazi and Whitson.³³ This procedure involved the knowledge of critical properties and the acentric factor of the substances, which were collected or estimated from literature studies.^{28,34–36}

For scenario (2), i.e. when the reactor is filled with Raschig rings, the radial mass dispersion coefficient was determined by eq (47).³⁷

$$d_{\mathrm{disp},i}^{j} = v_{z}^{\mathrm{ave}} D_{\mathrm{RR}} / (\varepsilon_{\mathrm{RR}} P e_{\mathrm{RR}}) \tag{47}$$

where ε is the porosity, Pe is the Péclet number and the subscript RR refers to the Raschig rings. The Péclet number for the scenario with Raschig rings was determined by eq (48).³⁷

$$1/Pe_{RR} = 1/[9 - 3.3 \exp(-7/Re_{RR})] + \varepsilon_{RR}/(\tau_{RR}Re_{RR}Sc_{RR})$$
(48)

The Reynolds number (Re) and the Schmidt number (Sc) for the scenario with Raschig rings were determined by eqs (49) and (50).³⁷

$$Re_{\rm RR} = v_z^{\rm ave} D_{\rm RR} / v \tag{49}$$

$$Sc_{RR} = v/d_{\text{diff},i}^{j} \tag{50}$$

The apparent kinematic viscosity of the biphasic system (ν) was estimated based on the expression derived from our previous work (eq(51)).¹¹

$$v\left[\text{m}^2\cdot\text{s}^{-1}\right] = \left[1.45 + (4.18 + 0.0653 N\left[\text{s}^{-1}\right])X\right] \times 10^{-6} \exp\left[170/(T\left[\text{K}\right] - 273.15)\right]$$
 (51)

The double bond conversion was calculated with eq(52).

$$X = 1 - c_{\mathrm{DB}}^{\mathrm{org}}/c_{\mathrm{DB},0}^{\mathrm{org}} \tag{52}$$

Eq (51) is also dependent on the stirring speed (N), since it was derived considering a stirring tank. An equivalent value for the stirring speed was estimated for the present study, as a function of the Sauter mean diameter of the dispersed phase (D_{32}), leading to eq(53). This empirical correlation was obtained based on the expression of Khakpay et al.³⁸ and the data from our previous work.¹¹

$$N[s^{-1}] = 9.697 \times 10^{-3} (D_{32} [m])^{-0.8223}$$
(53)

The value of the global heat transfer coefficient was estimated considering the external resistances associated with the heat transfer fluid and the pipe walls, according to eq (54).

$$U_{\text{ext}} = 1/(e_{\text{wall}}/\lambda_{\text{wall}} + 1/h_{\text{ext}}) \tag{54}$$

in which the wall thickness (e_{wall}) was assumed to have a constant value of 3.5 mm, and the heat transfer coefficient of the external fluid (h_{ext}) was estimated to be 766.14 W·m⁻²·K⁻¹, according to our previous study.¹¹

The thermal conductivity related to the pipe walls was described by eq (55), as a function of the temperature.³⁹

$$\lambda_{\text{wall}} \left[W \cdot m^{-1} \cdot K^{-1} \right] = 7.9318 + 2.0351 \times 10^{-2} \ T \left[K \right] - 6.4166 \times 10^{-6} \ (T \left[K \right])^2$$
 (55)

The volumetric interfacial area was determined by eq(56), assuming that the dispersed aqueous phase presents a spherical shape, with D_{32} as the Sauter mean diameter.

$$a_{\rm V} = 6/D_{32}$$
 (56)

The Sauter mean diameter was estimated by using different correlations, depending on the case analyzed. Eq (57) describes the correlation used for the cases with no static mixers and for the cases in which the reactor was filled with Raschig rings as static mixers. This equation is valid for a laminar-viscous shear flow.⁴⁰

$$D_{32} = 2\sigma W e_{\rm cr} / (\mu^{\rm org} S) \tag{57}$$

where We_{cr} is the critical Weber number, S is the shear rate, and σ is the interfacial tension between the phases, considered to be $0.02 \text{ N} \cdot \text{m}^{-1}$.³¹

Eq (58) is an empirical correlation, based on literature data, 40,41 in which the critical Weber number can be estimated as a function of the viscosity ratio between the dispersed and continuous phases. This correlation was described considering values within the range $0.0001 \le \mu^{aq}/\mu^{org} \le 0.1$.

$$We_{\rm cr} = 0.2441(\mu^{\rm aq}/\mu^{\rm org})^{-0.4008} \tag{58}$$

The shear rate was assumed to be an average value of the velocity gradient, determined by eq(59), in which v_z^{ave} is the average value for the velocity and D_h is the hydraulic diameter.

$$S = 4v_z^{\text{ave}}/D_{\text{h}} \tag{59}$$

The cases that employed SMX static mixers used eq (60) as the correlation to estimate the Sauter mean diameter, in which the subscript sm refers to these static mixers.²¹

$$D_{32}/D_{\text{SMX}} = 0.29We_{\text{SMX}}^{-0.2}Re_{\text{SMX}}^{-0.16} \tag{60}$$

The Weber number (We_{sm}) and the Reynolds number (Re_{sm}) for the SMX static mixers were calculated from eqs (61) to (62).

$$We_{\rm SMX} = \rho^{\rm ave} D_{\rm SMX} (\tau_{\rm SMX} v_z^{\rm ave})^2 / (\varepsilon_{\rm SMX}^2 \sigma)$$
(61)

$$Re_{\rm SMX} = D_{\rm SMX} \tau_{\rm SMX} v_z^{\rm ave} / (\varepsilon_{\rm SMX} v) \tag{62}$$

where ε is the porosity and τ is the tortuosity related to the static mixer.

The pressure drop (ΔP) was also estimated using different correlations for each case. For the cases in the absence of static mixers, the pressure drop was estimated with eq(63).⁴²

$$\Delta P_{\rm t} = 2f_{\rm t} \rho^{\rm ave} (v_{\rm z}^{\rm ave})^2 L_{\rm t} / D_{\rm t} \tag{63}$$

in which f is the friction factor, L is the length, and the subscript t refers to the pipe. The pipe length was estimated for each case according to an average residence time of 2 h for the reaction system inside the reactor.

For a laminar flow, the friction factor associated with the pipe can be calculated from eq (64):

$$f_{\rm t} = 16/Re_{\rm t} \tag{64}$$

The Reynolds number associated with the flow in a pipe in the absence of static mixers was calculated as eq(65).

$$Re_{\rm t} = v_{\rm z}^{\rm ave} D_{\rm t} / v \tag{65}$$

In the cases that considered the reactor filled with Raschig rings as static mixers, the pressure drop was calculated from the Ergun equation, eq (66), expressed in SI units.⁴³

$$\frac{\mathrm{d}P_{\mathrm{RR}}}{\mathrm{d}z} = \frac{G(1 - \varepsilon_{\mathrm{RR}})}{\rho^{\mathrm{ave}}\Phi_{\mathrm{RR}}D_{\mathrm{RR}}\varepsilon_{\mathrm{RR}}^3} \left[\frac{150(1 - \varepsilon_{\mathrm{RR}})\rho^{\mathrm{ave}}v}{\Phi_{\mathrm{RR}}D_{\mathrm{RR}}} + 1.75G \right] \tag{66}$$

where the subscript R refers to the Raschig rings.

The mass flux G was calculated from eq (67), in which m is the total mass flow rate.

$$G = 4m/\pi D_t^2 \tag{67}$$

Lastly, for the cases using the SMX static mixers, the pressure drop was calculated from eq (68).²¹

$$\Delta P_{\rm SMX} = 2f_{\rm SMX} \rho^{\rm ave} (v_z^{\rm ave})^2 L_{\rm SMX} \tau_{\rm SMX}^3 / (\varepsilon_{\rm SMX}^2 D_{\rm SMX})$$
 (68)

The friction factor related to the SMX static mixers was calculated with eq(69).²¹

$$f_{\rm SMX} = 16/Re_{\rm SMX} + 0.1936 \tag{69}$$

Two important properties concerning the epoxidation of vegetable oils are the iodine and the oxirane indexes. The iodine index (II) is a value proportional to the concentration of double bonds of the oil and is defined as the amount of I_2 that reacts with all the remaining double bonds of a sample of 100 g of oil. The oxirane index (OI) measures the weight percentage of oxirane oxygen atoms in the epoxidized oil.¹¹ These properties can be determined from eqs (70) and (71).

$$II = 100c_{\mathrm{DB}}^{\mathrm{org}} M_{\mathrm{I}_2} / \rho^{\mathrm{org}} \tag{70}$$

$$OI = 100c_{\rm EG}^{\rm org}M_{\rm O}/\rho^{\rm org} \tag{71}$$

in which M is the molar mass, and the subscripts I_2 and O refer to the iodine molecule and the oxirane oxygen atom.

The constant parameters of the present model are summarized in Table 5.

Table 5. Parameters collected from the literature and experimental conditions.

Parameter	Value	Unit	Reference
$k_{1,r}^{\text{aq}} \text{ at } T_{\text{r}} = 70 ^{\text{o}}\text{C}$	5.49×10 ⁻³	L ² ·mol ⁻² ·s ⁻¹	11
$k_{2,\mathrm{r}}^{\mathrm{aq}}$ at $T_{\mathrm{r}} = 70$ °C	2.00×10 ⁻⁴	s ⁻¹	11
$k_{1,\mathrm{r}}^{\mathrm{org}}$ at $T_{\mathrm{r}} = 70 {}^{\mathrm{o}}\mathrm{C}$	7.30×10 ⁻²	$L \cdot mol^{-1} \cdot s^{-1}$	11
$k_{2,\mathrm{r}}^{\mathrm{org}}$ at $T_{\mathrm{r}} = 70 \mathrm{^oC}$	3.43×10 ⁻⁸	$L^2 \cdot m \cdot mol^{-2} \cdot s^{-1}$	11
$k_{3,\mathrm{r}}^{\mathrm{org}}$ at $T_{\mathrm{r}} = 70 \mathrm{^oC}$	2.90×10 ⁻⁷	$L^2{\cdot}m{\cdot}mol^{\text{-}2}{\cdot}s^{\text{-}1}$	11
$k_{4,\mathrm{r}}^{\mathrm{org}}$ at $T_{\mathrm{r}} = 70 \mathrm{^oC}$	1.43×10 ⁻⁹	$L^2{\cdot}m{\cdot}mol^{\text{-}2}{\cdot}s^{\text{-}1}$	11
$k_{5,\mathrm{r}}^{\mathrm{org}}$ at $T_{\mathrm{r}} = 70 \mathrm{^oC}$	4.78×10 ⁻⁹	$L^2{\cdot}m{\cdot}mol^{\text{-}2}{\cdot}s^{\text{-}1}$	11
$E_1^{ m aq}$	5.09×10 ⁴	J·mol¹¹	11
$E_2^{ m aq}$	9.75×10^4	J·mol¹¹	11
E_1^{org}	3.80×10^4	J·mol¹¹	11
E_2^{org}	4.75×10 ⁴	J·mol¹¹	11
E_3^{org}	9.54×10^4	J·mol¹¹	11
$E_4^{ m org}$	5.85×10 ⁴	J·mol¹¹	11
E_5^{org}	2.87×10^4	J·mol¹¹	11
${\pmb \beta}^{\rm aq}$	5.30×10 ⁻⁵	m·s ⁻¹	11
$K_{1,\rm r}^{\rm aq}$ at $T_{\rm r} = 70~{\rm ^{o}C}$	0.95		10

ΔH_1^{aq}	-10781	J·mol⁻¹	Estimated from ref ¹⁰
$\Delta H_2^{ m aq}$	-235478	J·mol ⁻¹	Estimated from ref 44,45
$\Delta H_1^{\mathrm{org}}$	-174723	J·mol ⁻¹	Estimated from ref ⁴⁴
$\Delta H_2^{\mathrm{org}}$	37710	J·mol⁻¹	Estimated from ref 44
$\Delta H_3^{\mathrm{org}}$	37710	J·mol⁻¹	Estimated from ref 44
$\Delta H_4^{ m org}$	12570	J·mol⁻¹	Estimated from ref 44
$\Delta H_5^{\mathrm{org}}$	12570	J·mol⁻¹	Estimated from ref 44
σ	0.02	$N \cdot m^{-1}$	31
$M_{ m I_2}$	253.8	g·mol⁻¹	
$M_{ m O}$	16.0	g·mol⁻¹	
m	0.278	kg·s ⁻¹	
w^{org}	0.685		
$w^{ m aq}$	0.315		
$h_{ m ext}$	766.14	$W \cdot m^{-2} \cdot K^{-1}$	Estimated from ref 11
$T_{ m ext}$	313.15-	K	
	333.15		
$e_{ m wall}$	3.5×10 ⁻³	m	
$D_{ m t}$	2.66×10 ⁻² -	m	
	5.25×10 ⁻²		
D_{RR}	3.48×10 ⁻³	m	
$arepsilon_{ m RR}$	0.730		
$ au_{ m RR}$	1.8		37
$oldsymbol{arPhi}_{RR}$	0.384		
$D_{ m SMX}$	3.2×10 ⁻³	m	21

$arepsilon_{ ext{SMX}}$	0.77		21	
$L_{ m SMX}$	1.45×10 ⁻²	m	21	
$ au_{ m SMX}$	1.5		21	
$c_{ m FA,0}^{ m aq}$	2.88	$mol \cdot L^{-1}$		
$c_{ m HP,0}^{ m aq}$	18.33	$mol \cdot L^{-1}$		
$c_{ m PFA,0}^{ m aq}$	0	$mol \cdot L^{-1}$		
$c_{ m W,0}^{ m aq}$	24.37	mol·L ⁻¹		
$c_{ ext{PFA},0}^{ ext{org}}$	0	mol·L ⁻¹		
$c_{\mathrm{DB,0}}^{\mathrm{org}}$	4.54	mol·L ⁻¹		
$c_{ m FA,0}^{ m org}$	0	mol·L ⁻¹		
$c_{ m EG,0}^{ m org}$	0	mol·L ⁻¹		
T_0	333.15	K		

3. Results and Discussion

The main results from the simulations of the epoxidation reaction of soybean oil in conventional tubular reactors are outlined in the present section.

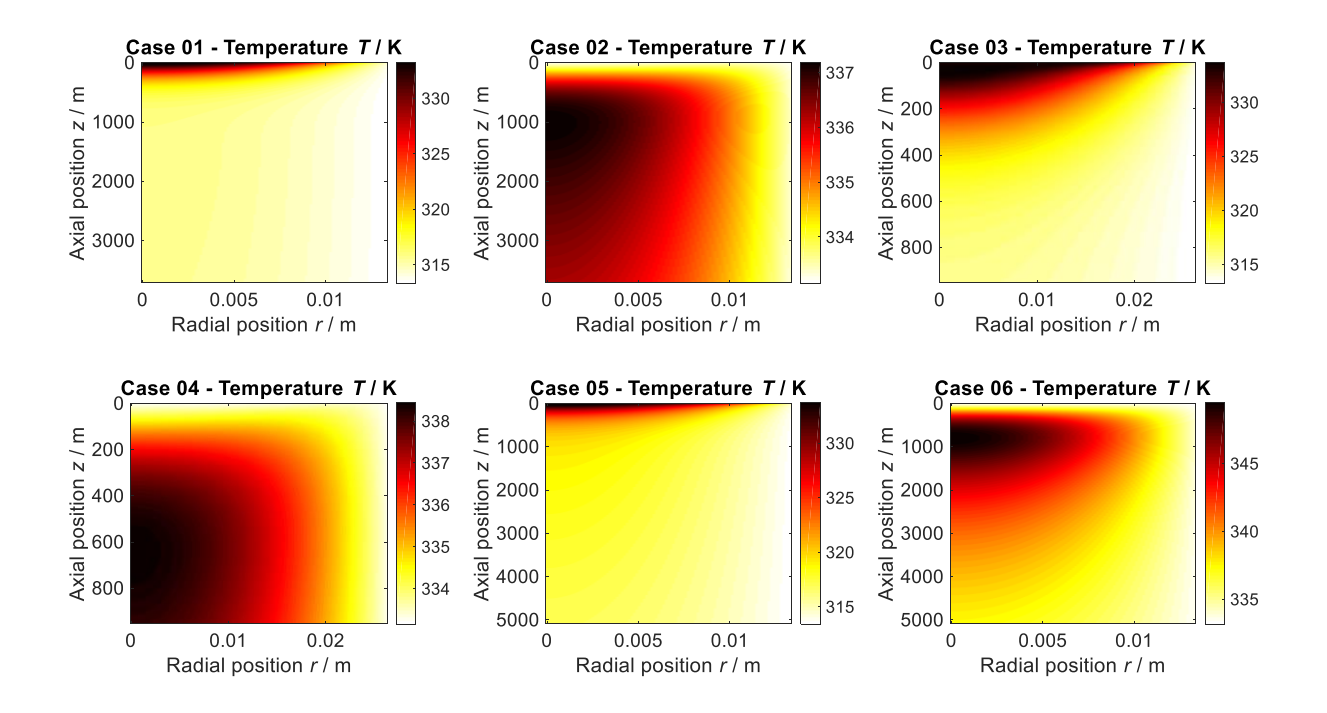
Table 6 summarizes: the ranges for the Sauter mean diameter (D_{32}) and volumetric interfacial area (a_V); the maximum temperature (T_{max}); the average values for the iodine index (II_f), oxirane index (OI_f), and pressure drop (ΔP_f) at the exit of the reactor; and the pressure drop for the segments of the reactor (ΔP_{seg}) for cases 09-17. Figure 3 provides the temperature profiles inside the reactor, while Figures 4-6 show a comparison between the maximum temperature, exit iodine index and exit oxirane index values achieved in each case. Figures 7-8 present the behavior of the

average values of the iodine and oxirane indexes, respectively, along the tubular length. Figure 9 provides the average values of the pressure drop as a function of the tubular length.

Table 6. Main results of the simulations of tubular reactors.

Case	D ₃₂ /	<i>a</i> _V /	T _{max} /	$II_{ m f}$ /	OI _f /	$\Delta P_{ m f}$ /	$\Delta P_{ m seg}$ /
	m	m ⁻¹	K	g I ₂ /(100 g)	%	Pa	Pa
01	3.15×10 ⁻²	1.91×10 ²	333.28	104.03	1.57	2.58×10 ⁷	
02	3.15×10 ⁻²	1.91×10^{2}	337.19	100.40	1.79	7.52×10^{6}	
03	2.42×10 ⁻¹	2.48×10^{1}	333.74	124.10	0.31	2.70×10 ⁵	
04	2.42×10 ⁻¹	2.48×10^{1}	338.43	124.51	0.28	6.63×10 ⁴	
05	2.05×10 ⁻³	2.93×10^{3}	333.70	69.07	3.76	5.05×10^{10}	
06	2.05×10 ⁻³	2.93×10^{3}	349.48	24.59	6.49	2.52×10^{10}	
07	8.50×10 ⁻³	7.06×10^{2}	339.29	75.69	3.35	6.01×10^{8}	
08	8.50×10 ⁻³	7.06×10^{2}	378.41	72.68	3.53	2.50×10^{8}	
09	6.13×10 ⁻⁵ –	6.97×10 ⁴ –	335.68	50.98	4.05	2.86×10^{7}	3.41×10^6 –
	8.61×10 ⁻⁵	9.79×10^{4}					1.05×10^7
10	6.13×10 ⁻⁵ –	7.92×10 ⁴ –	391.72	22.17	4.33	1.37×10^{7}	1.59×10 ⁶ –
	7.58×10 ⁻⁵	9.79×10^{4}					4.42×10^{6}
11	1.25×10 ⁻⁴ –	3.42×10 ⁴ –	459.51	53.03	3.42	3.99×10 ⁵	1.82×10 ⁴ –
	1.76×10 ⁻⁴	4.81×10 ⁴					2.19×10 ⁵
12	1.25×10 ⁻⁴ –	3.99×10 ⁴ –	470.77	57.24	3.04	1.68×10 ⁵	1.76×10 ⁴ –
	1.50×10 ⁻⁴	4.81×10^4					6.72×10 ⁴
13	1.26×10 ⁻⁴ –	3.16×10 ⁴ –	454.23	49.08	3.57	6.50×10 ⁵	$9.33 \times 10^3 -$
	1.90×10 ⁻⁴	4.90×10 ⁴					1.60×10 ⁵

14	1.24×10 ⁻⁴	-3.07×10^{4}	- 434.14	38.67	4.21	1.24×10 ⁶	7.66×10 ³ –
	1.95×10 ⁻⁴	4.83×10^4					1.42×10 ⁵
15	1.28×10 ⁻⁴	-3.03×10^{4}	- 401.80	24.09	5.24	1.86×10^{6}	8.66×10^3 –
	1.98×10 ⁻⁴	4.67×10 ⁴					1.36×10 ⁵
16	1.31×10 ⁻⁴	-3.05×10^4	- 368.97	18.39	5.92	2.28×10 ⁶	1.00×10 ⁴ –
	1.96×10 ⁻⁴	4.57×10 ⁴					1.22×10 ⁵
17	1.31×10 ⁻⁴	-3.10×10^{4}	- 350.71	21.43	5.95	2.65×10 ⁶	9.73×10 ³ –
	1.94×10 ⁻⁴	4.57×10 ⁴					1.07×10 ⁵



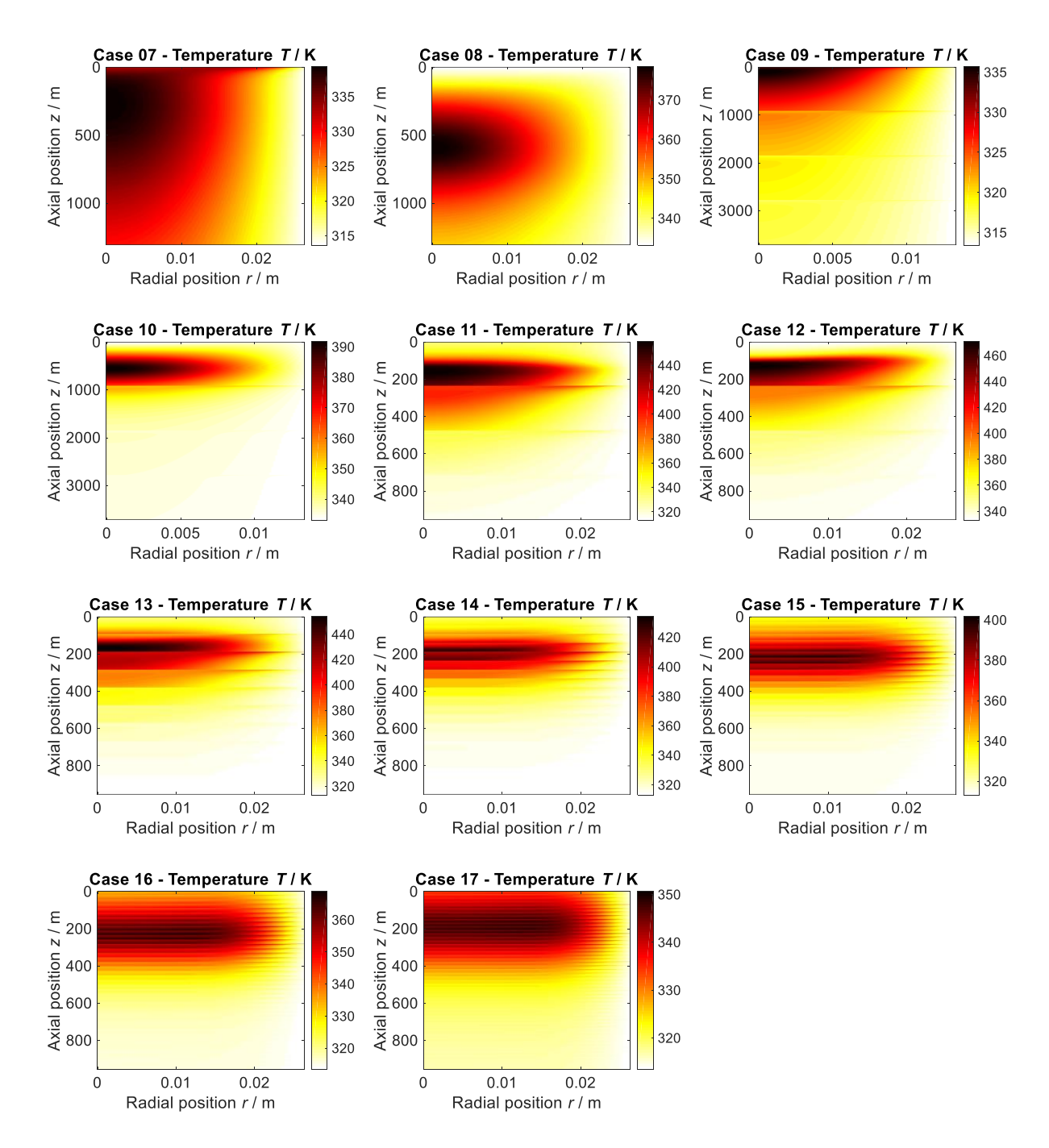


Figure 3. Temperature profiles as a function of the radial and axial positions in the tubular reactor for the cases studied.

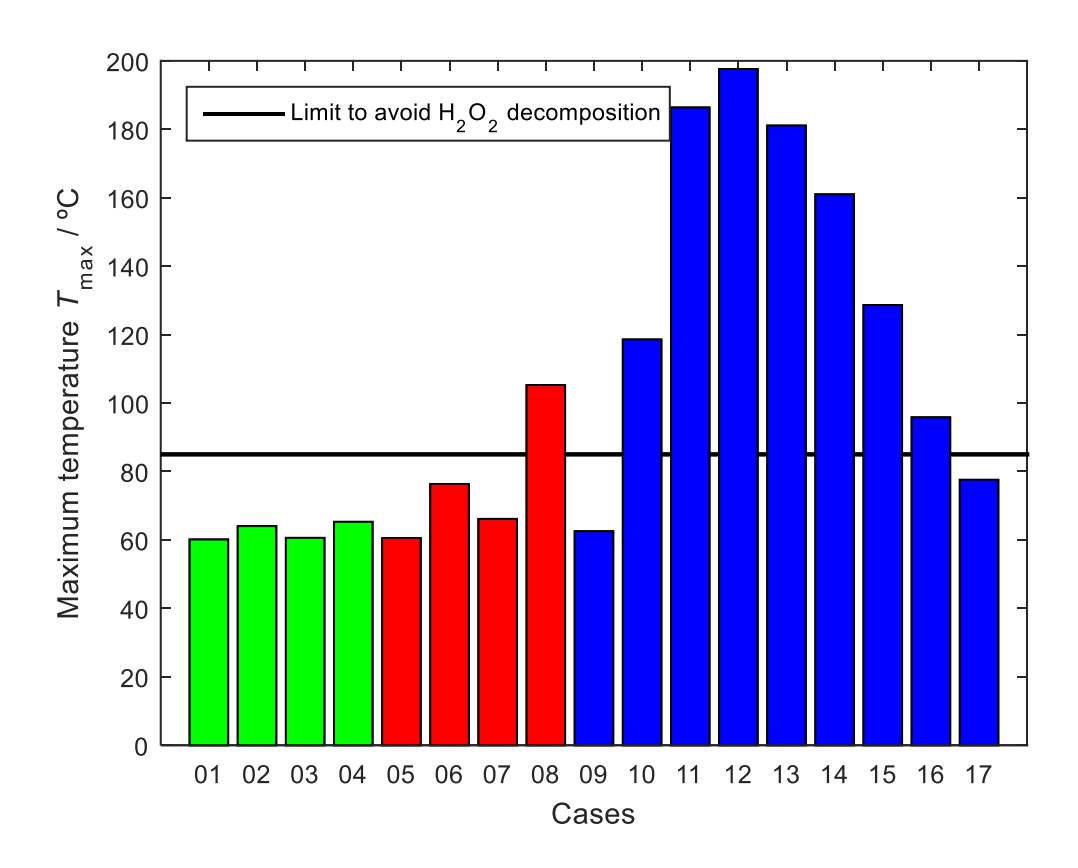


Figure 4. Comparison between the maximum temperature results for the cases studied: green bars refer to the cases without static mixers; red bars refer to the use of Raschig rings; blue bars refer to the use of Sulzer SMXTM static mixers.

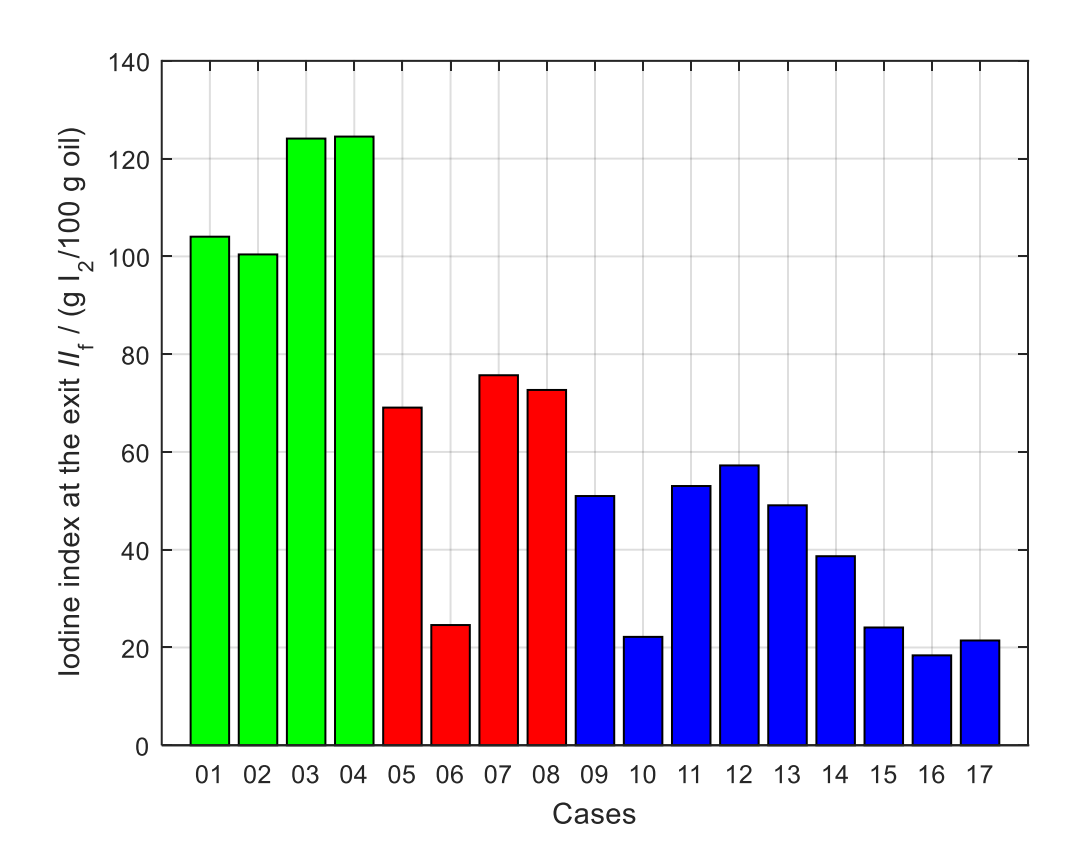


Figure 5. Comparison between the iodine index values for the cases studied: green bars refer to the cases without static mixers; red bars refer to the use of Raschig rings; blue bars refer to the use of Sulzer SMXTM static mixers.

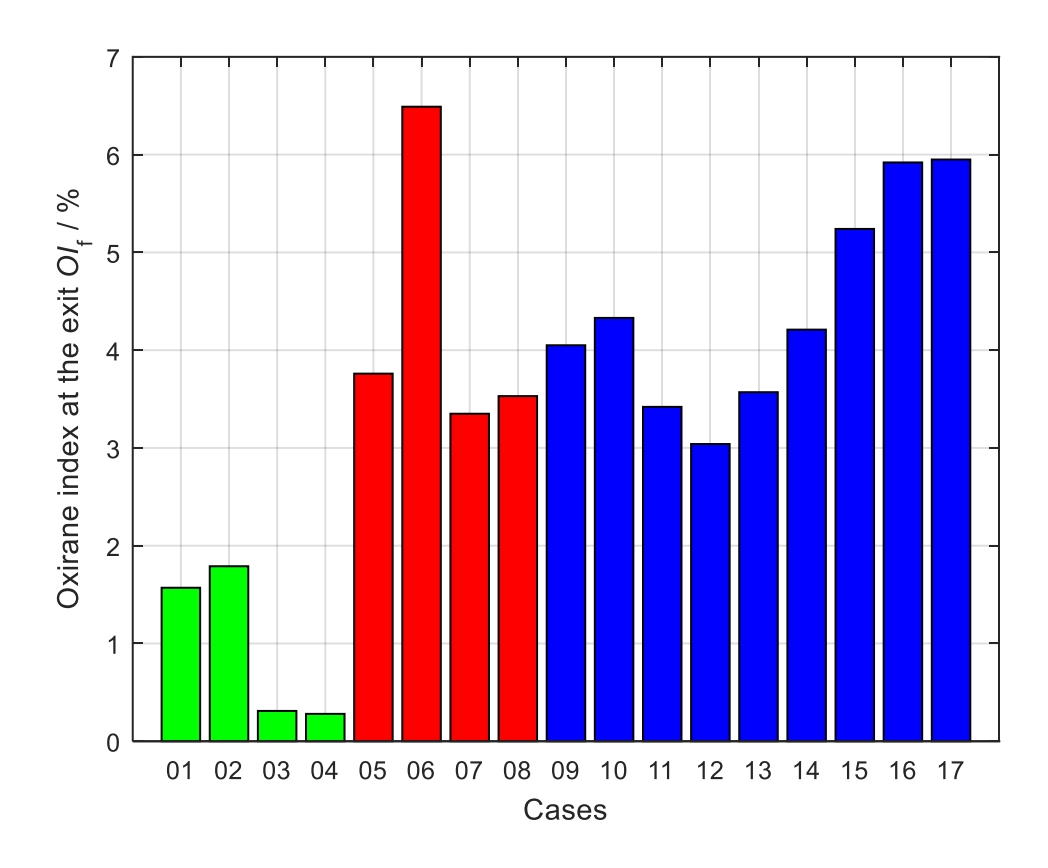


Figure 6. Comparison between the oxirane index values for the cases studied: green bars refer to the cases without static mixers; red bars refer to the use of Raschig rings; blue bars refer to the use of Sulzer SMXTM static mixers.

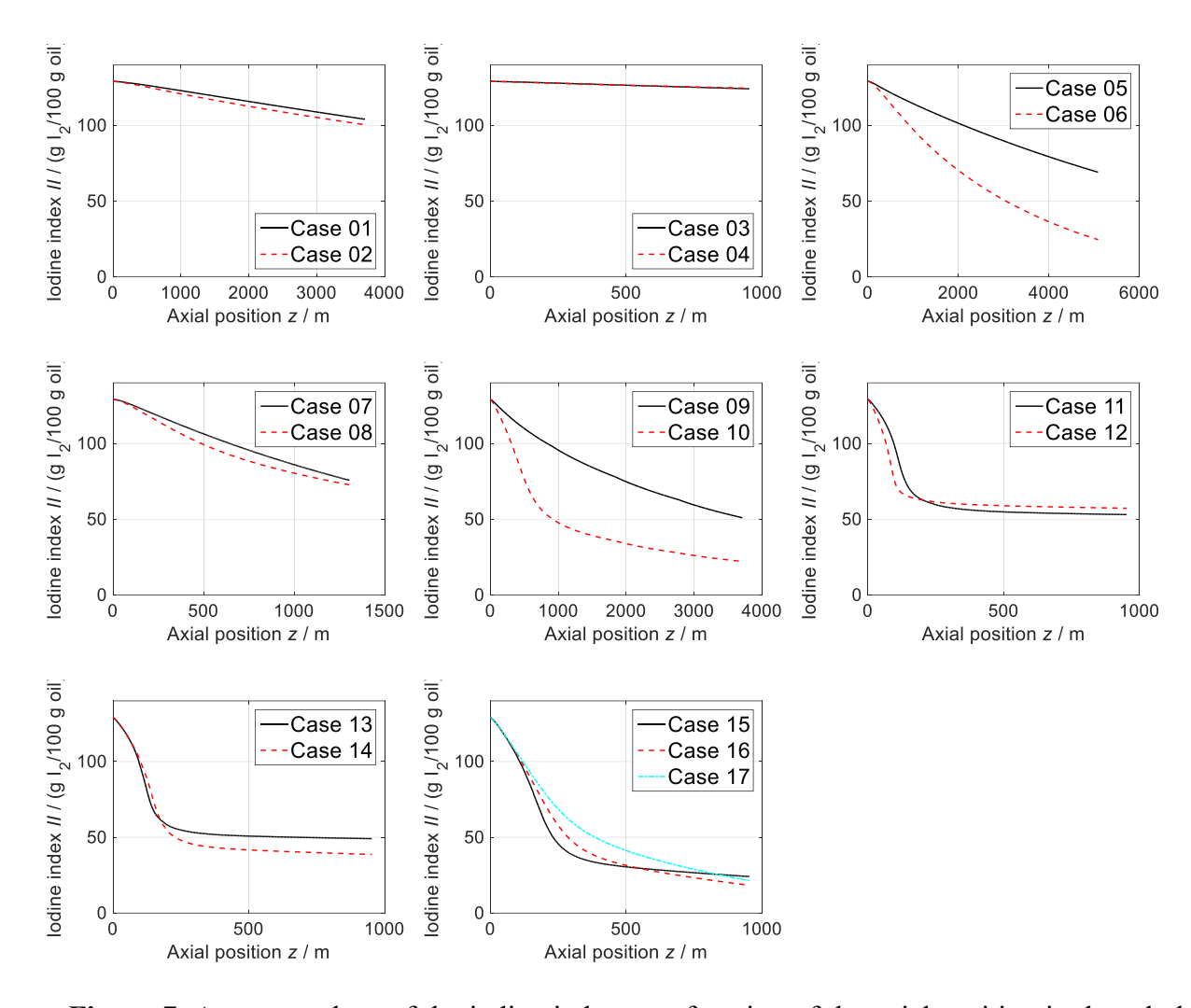


Figure 7. Average values of the iodine index as a function of the axial position in the tubular reactor for the cases studied.

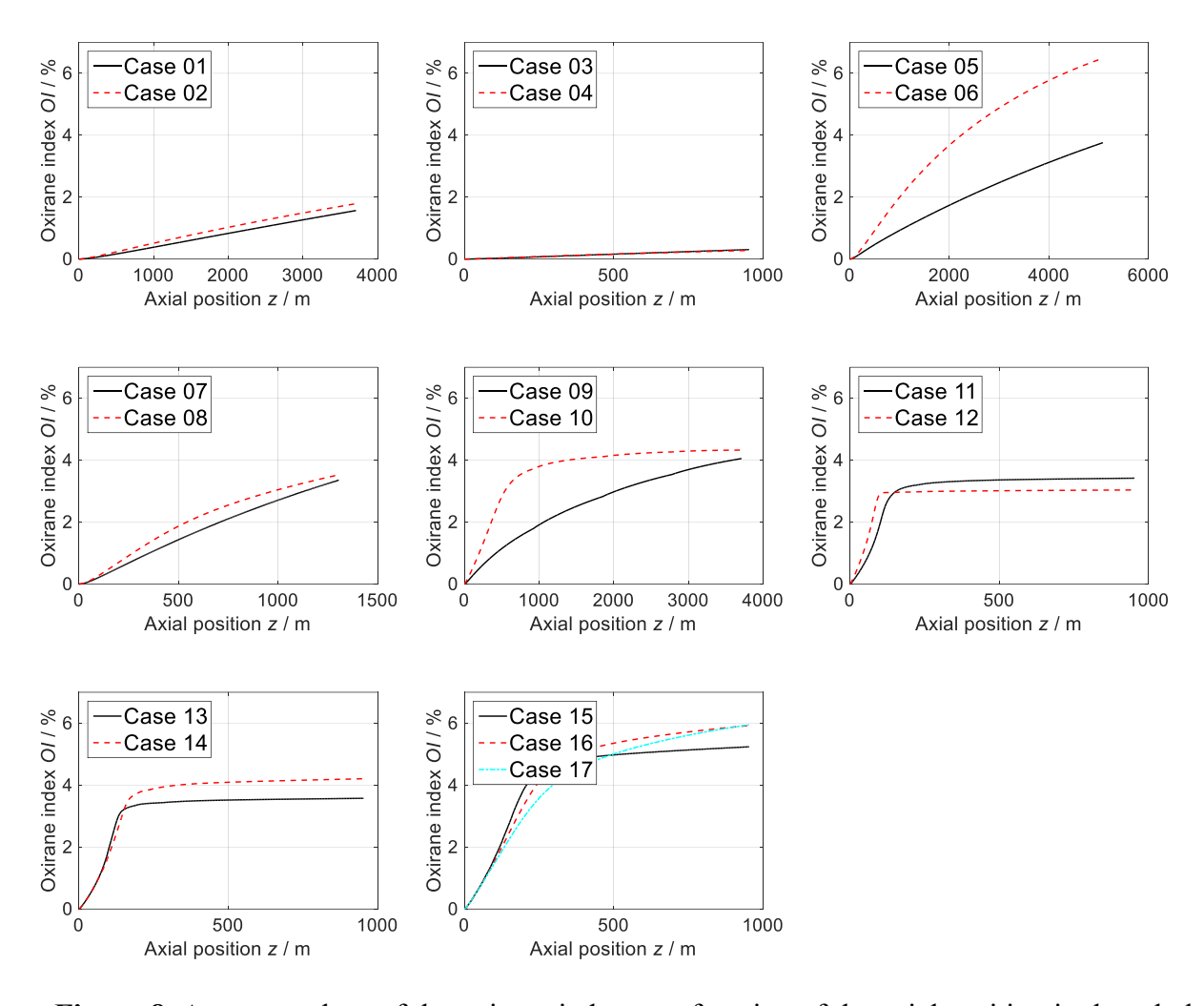


Figure 8. Average values of the oxirane index as a function of the axial position in the tubular reactor for the cases studied.

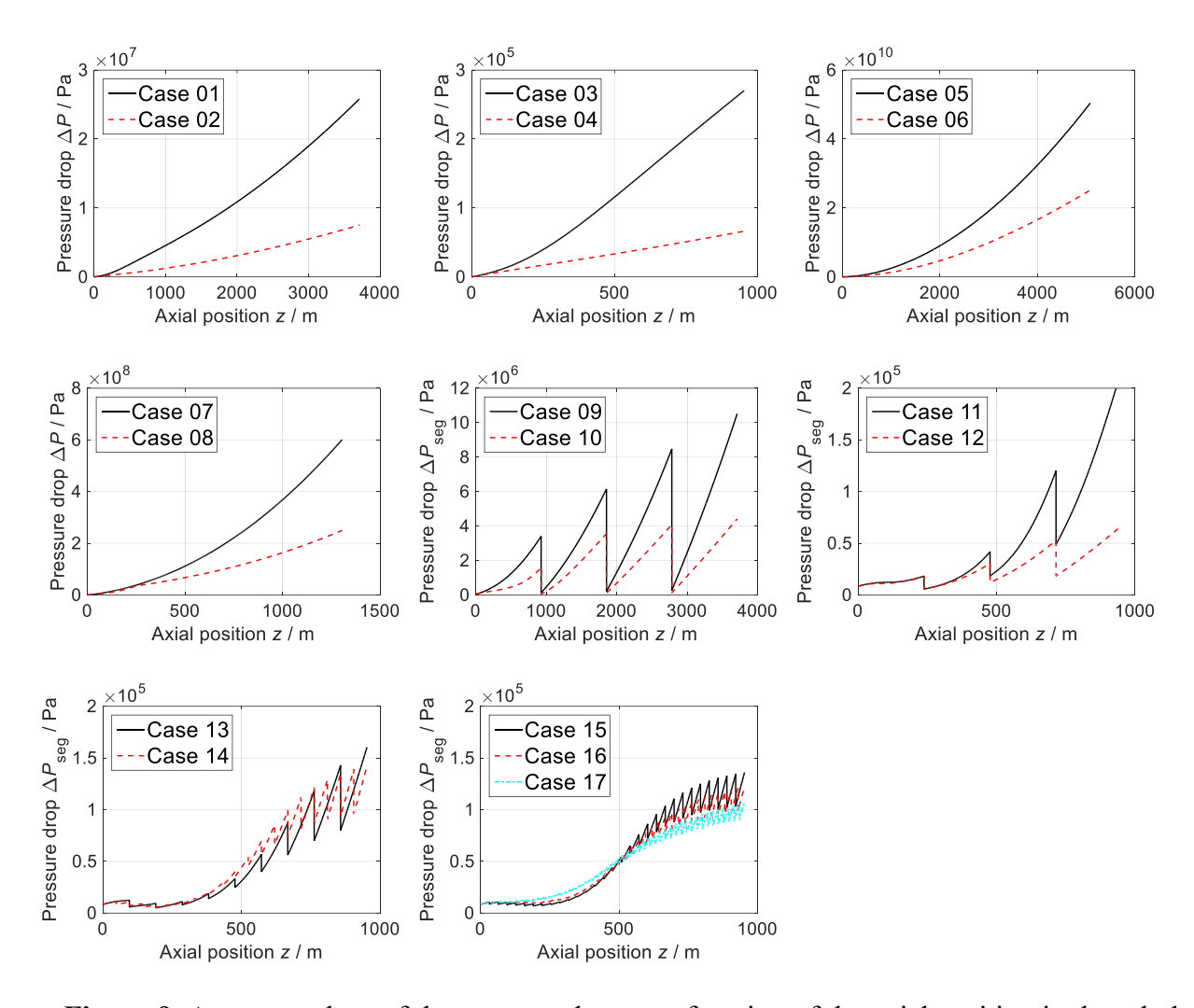


Figure 9. Average values of the pressure drop as a function of the axial position in the tubular reactor for the cases studied.

Clearly, the use of static mixers is essential under the proposed conditions, in order to assure an adequate interfacial area per unit volume for the reaction system to operate properly. Cases 01-04, which simulated operations of the reactor in the absence of static mixers, resulted in the lowest values for this property, in accord with the highest values for the Sauter mean diameter. One explanation for this is that, under laminar flow conditions, there is insufficient shear between the fluid layers to maintain the dispersed phase of the system as small droplets. Moreover, it is important to emphasize that the estimated values of D_{32} for these cases surpass the corresponding

values of the pipe diameter, suggesting a tendency of coalescence of the dispersed phase droplets, leading to a slug flow.

The values of the interfacial area per unit volume for cases 01-04 can also be considered insufficient for the proposed conditions when one analyzes the respective final values of the iodine and oxirane indexes. The decrease in the iodine index is associated with the corresponding increase in the conversion of the soybean oil double bonds. Considering that the iodine index for pure soybean oil is 129 g I₂/(100 g oil), relatively low conversion values would be achieved under these conditions. Consequently, the oxirane index values were also low, considering that the theoretical maximum value of this property is expected to be 7.52%. Evidently, these results derive from the low contact area between the phases, limiting mass transfer and, consequently, the main reaction in the organic phase (epoxidation reaction). This mass transfer limitation leads to the observed low heat generation rate.

Conversely, the simulations in which the reaction was conducted in the presence of static mixers (cases 05-17) resulted in lower values for the Sauter mean diameter of the dispersed phase, due to the significant increase in the shear associated with the friction of the fluid with the static mixers. Hence, higher values of the interfacial area per unit volume were estimated for these cases, resulting in an intensification of the mass transfer effects and the epoxidation reaction. Therefore, a decrease in II_f and an increase in OI_f can be expected in these situations, as well as an increase in the heat generation rate due to the epoxidation reaction.

The intensification of the heat generation rate can cause a temperature overshoot, which can vary depending on the tube diameter and the external temperature. The larger the tube diameter, the higher the tendency for a temperature overshoot, since the heat transfer resistance increases in this

situation. More intuitively, as the temperature of the external fluid increases, the heat removal rate from the reaction medium tends to diminish.

The maximum temperature is an important value to be considered for the epoxidation of vegetable oils. This value is mainly affected by the balance between the heat generation rate by the exothermic reactions and the heat removal rate. When this value is not properly evaluated and controlled, this can induce undesirable effects on the reaction media, such as the hydrogen peroxide decomposition, which can compromise the security of the process, as stated in our previous study. Di Serio et al. Mention that the decomposition reaction of hydrogen peroxide usually occurs at temperatures above 90 °C (363.15 K), while the study of Santacesaria et al. The presented results that point to the significance of this decomposition at 85 °C (358.15 K) for a pH of 3.5 with stainless steel as a catalyst. Besides the consumption of a key reactant in the epoxidation reaction system, the decomposition of hydrogen peroxide also generates large volumes of oxygen, which may compromise the security of the process. The model proposed in the present study did not include a quantification of this reaction, because the aim is precisely to avoid reaching temperatures higher than the limit of 85 °C, when this undesired reaction occurs at considerable rates. Figure 4 indicates the value of 85 °C with the intent of specifying the limit that the temperature should not surpass.

For cases 09-17, in which the simulations included the SMX static mixers, the temperature overshoot can be minimized by allocating a greater number of static mixers along the reactor. Apart from providing the shear rate required to diminish the droplet size of the dispersed phase, an enhancement of the heat transfer is also expected from the use of the static mixers, which intensify the radial distribution of energy. Therefore, the maximum temperature tends to decrease as the number of SMX static mixers increases, evidenced by the comparison of cases 12 and 14-17. Furthermore, additional stations with static mixers may provide an additional safety layer since

the reactor is divided into shorter tubing sections that can be assembled to function as relief points in the case of a drastic and otherwise potentially catastrophic hydrogen peroxide decomposition.

The use of Raschig rings can also minimize the problem related to the temperature overshoot, acting as static mixers (cases 05-08) that fill the whole reactor and tend to intensify both heat and mass transfer effects.

Case 06 resulted in the highest value for the oxirane index at the reactor exit (6.49 %). The explanation for this high value may be related to the temperature behavior (Figure 2) and the droplet size. A temperature overshoot can be observed for this case, in which a maximum value of 349.48 K was achieved, corroborated by the external temperature of 333.15 K. Nevertheless, the temperature range within which the reaction was conducted in this case apparently prioritized the main reactions over the undesired ring-opening reactions and performic acid degradation. Moreover, the droplet size associated with this case (2.05×10⁻³ m) apparently favored the mass transfer effects on the main reactions, without significantly intensifying the interfacial ring-opening reactions.

Cases 10, 15, 16 and 17 resulted in similar values for the iodine index in the reactor exit stream, although the oxirane indexes were considerably different. The explanation for this discrepancy may be due to the same reasons described in the previous paragraph, i.e., the Sauter mean diameter and the temperature profile. The conditions for cases 10, 15, 16, and 17 resulted in a droplet diameter that was an order of magnitude smaller than that in case 06. These smaller values for the droplet diameter would significantly intensify the mass transfer effects, the main reactions, and the interfacial ring-opening reactions. The intensification of the epoxidation reaction leads to a greater heat generation rate, which increases the temperature overshoot. Besides contributing to hydrogen peroxide decomposition, the increase in temperature should affect the oxirane ring-opening

reaction more than the other reactions, since this undesired reaction has the highest activation energy. Therefore, the conditions for cases 10, 15, 16, and 17 tend to favor the oxirane ring opening more than case 06. Nevertheless, the inclusion of a greater number of SMX static mixers in the reactor tended to minimize the temperature overshoot, since the mixing of the system promoted by the static mixers intensifies the radial heat transfer effects.

Additionally, according to Figures 7-8, the iodine and oxirane indexes for cases 11-14 remained almost constant along the major part of the reactor. This may have happened due to the increase in temperature in the initial portion of the reactor, which benefited the performic acid decomposition, leading to the high consumption of formic acid. Therefore, after the reaction media flows through this initial section, the lack of formic acid considerably decreases the main reactions rates, leading to the apparently constant values for the iodine and oxirane indexes in the model. It is important to emphasize that this problem may be reduced by the addition of more static mixers.

Concerning the pressure effects, the absence of static mixers (cases 01-04) resulted in the lowest pressure drop values compared to the other cases with the same tube diameter. This was an expected outcome since the static mixers provide greater friction with the fluid. A lower pressure drop is beneficial from a cost point of view because the pumping requirements are reduced. Nonetheless, although the absence of static mixers presents this cost advantage, it would be impractical to conduct the reaction under these conditions with a residence time of 2 h, due to the mass transfer limitations previously noted.

Comparing the cases using Raschig rings (cases 05-08) with those for the same tube diameter using SMX static mixers (cases 09-17), it is noteworthy that the use of Raschig rings throughout the whole reactor results in a pressure drop that is orders of magnitude higher than that with SMX static mixers positioned at locations along the reactor. As mentioned previously, the conditions of

case 06 led to promising results, based on the highest value of the oxirane index. Nonetheless, the pressure drop associated with this case is 2.52×10^{10} Pa, approximately 248705 times atmospheric pressure. This elevated value for the pressure drop derives from the friction of the fluid with the Raschig rings along the entire length of the reactor (5084 m), the highest among the analyzed cases. Therefore, despite the promising results concerning the reaction yield in case 06, it would be impractical to conduct the reaction under the proposed conditions.

Aiming at reducing the extremely high values of the pressure drop, instead of carrying out the reaction in a series configuration in a long tubular reactor, it could be performed in a parallel configuration consisting of several shorter pipes in which the reaction media could be subdivided. However, this scenario was not considered for simulation, because the velocity associated with the reaction media flow is expected to decrease to the point that shear effects could not maintain the droplets, leading to decantation.

Conversely, the use of SMX static mixers resulted in significantly lower values for the pressure drop compared to the use of Raschig rings. These values decreased for the cases in which the tube diameter was 2 in (cases 11-17), compared to those with a 1 in tube diameter (cases 09-10). The use of a tube with a larger diameter disfavors heat transfer with the external fluid, which tends to increase the temperature overshoot. The use of a greater number of static mixers should minimize this effect. The increase in the number of static mixers also enhances the pressure drop, but this value remains viable for application in a real scenario.

Therefore, case 17 shows the most promising results, since a considerable value of the interfacial area can be achieved, leading to a significant consumption of the soybean oil double bonds and formation of oxirane groups (based on the final values of 21.43 g I₂/(100 g oil) for the iodine index and 5.95% for the oxirane index), together with a controlled temperature range (maximum value

of 350.71 K) and a more viable pressure drop (2.65×10⁶ Pa, or 26.2 atm). If we consider the reduced heat generation at the reactor exit in case 17, it should be viable to design a tandem stirred tank reactor that would allow the reaction to reach the desired specification of a minimum 6.60 oxirane index.

Moreover, the use of more static mixers, i.e., the subdivision of the reactor into more segments in series, corroborates the hypothesis of considering a constant diameter for the dispersed phase. In practical terms, the use of static mixers may even not be necessary if a shear pump can be used to generate droplets of a significant size to avoid mass transfer limitations. However, the idea of the series reactor segments should be maintained in this case.

A final scenario that it is noteworthy to consider in case 17, for safety reasons, is related to a potential catastrophic hydrogen peroxide decomposition reaction. Table 6 shows a maximum temperature value of 77.56 °C for case 17, so hydrogen peroxide decomposition would not normally be expected to happen. Nevertheless, for safety considerations, it is important to assume potential failures in the process that could result in the system temperature surpassing 85 °C or other failures that could lead to rapid hydrogen peroxide degradation. Two of the experiments provided in our previous study showed that, when this happens, the system temperature can rapidly reach more than 150 °C. Considering the stoichiometry of the degradation reaction and the gas/vapor generation, the volumetric flow rate is expected to increase approximately 1840-fold. Assuming a worst-case scenario, i.e., this abrupt expansion occurring exactly in the middle of a tube segment, the calculated pressure drop predicted by eq (63) would lead to a value of 5714 Pa, which is well within the operational limits for the system. Therefore, this preliminary analysis suggests that, even in the adverse scenario of an abrupt hydrogen peroxide decomposition in case 17, the gases generated should be vented to the atmosphere without significantly compromising

the process safety. In the case of a practical application, it is important to note that these safety considerations would need to be reviewed and calculated in further detail and with greater accuracy.

4. Conclusions

The present study analyzed the viability of conducting the reaction of soybean oil epoxidation in a continuous tubular reactor with a residence time of 2 h, in the absence or presence of static mixers, based on the kinetic model proposed in our previous article. The simulations of the reactor in the absence of static mixers led to the economic advantage of low pressure drop. However, the low contact area between the phases makes this approach unfeasible in a real situation, due to mass transfer limitations. The use of Raschig rings throughout the entire reactor led to interesting results, due to the enhancement of mass and heat transfer effects. Nevertheless, the resulting elevated pressure drop makes the use of Raschig rings impractical. Lastly, the cases in which Sulzer SMXTM static mixers were employed proved to be potentially the most viable for a real scenario. In particular, the use of a 2 in diameter tube, with 50 static mixers distributed along the reactor and an external fluid at the temperature of 313.15 K, resulted in a controlled maximum temperature of 350.71 K, a pressure drop of 2.65×10⁶ Pa, and an effluent organic phase with iodine and oxirane indexes of 21.43 g I₂/(100 g oil) and 5.95%, respectively. Furthermore, the use of static mixers can be implemented so that they can also function as relief stations, separating the reactor into shorter segments, significantly improving the safety of the process and offering the opportunity to optimize the heat exchange conditions in each segment.

AUTHOR INFORMATION

Corresponding Author

*E-mail address: rgiudici@usp.br

Author Contributions

The manuscript was written through contributions of all authors. All authors have given approval to the final version of the manuscript.

ACKNOWLEDGMENT

This work was supported by the São Paulo Research Foundation (FAPESP, grant numbers 2019/00289-7 and 15/50684-9), the Conselho Nacional de Desenvolvimento Científico e Tecnológico (CNPq, grant numbers 140163/2019-0 and 309444/2016-0) and the Coordenação de Aperfeiçoamento de Pessoal de Nível Superior (CAPES, finance code 001). The authors also thank Prof. Frank Quina for revising the manuscript.

ABBREVIATIONS

Volumetric interfacial area (m⁻¹) av

Heat capacity (J·kg⁻¹·K⁻¹) C_p

Molar concentration (mol·L⁻¹) c

Diameter (m) D

Mass diffusion coefficient, mass dispersion coefficient (m²·s⁻¹) d

ESO Epoxidized soybean oil

EActivation energy (J⋅mol⁻¹)

Wall thickness (m) efFriction factor Н Partition coefficient Heat transfer convective coefficient (W·m⁻²·K⁻¹) hIodine index (g/100 g I₂) IIMass transfer molar rate per unit volume (mol·L⁻¹·s⁻¹) \boldsymbol{J} Equilibrium constant K k Kinetic constant LLength (m) Molar mass (g·mol⁻¹) MMass flow rate (kg·s⁻¹) mEquivalent stirring speed (s⁻¹) N Oxirane index (%) OI pK_a Logarithmic ionization constant of formic acid

•

Péclet number

Polyvinyl chloride

Reynolds number

Pe

PVC

Re

R Universal gas constant (J·mol⁻¹·K⁻¹)

Rate of reaction i in the phase j (mol·L⁻¹·s⁻¹)

Radial position (m)

S Shear rate (s⁻¹)

Sc Schmidt number

s Molecular radius (m)

Temperature (°C or K)

U Global heat transfer coefficient (W·m⁻²·K⁻¹)

v Velocity (m⋅s⁻¹)

We Weber number

w Mass fraction

X Conversion of the double bonds of soybean oil

z Axial position (m)

Greek symbol

 β Mass transfer coefficient (m·s⁻¹)

 ΔH Enthalpy of reaction (J·mol⁻¹)

 ΔP Pressure drop (Pa)

Porosity З Boltzmann constant κ Thermal conductivity $(W \cdot m^{-1} \cdot K^{-1})$ λ Dynamic viscosity (Pa·s) μ Apparent kinematic viscosity of the reaction system (m²·s⁻¹) v Density (kg·m⁻³) ρ Interfacial tension (N·m⁻¹) σ Tortuosity τ Φ Sphericity ϕ Volume fraction Subscripts and superscripts Aqueous phase aq Average value between the phases ave Critical value cr Double bonds of soybean oil DB diff Diffusion Dispersion disp

EG Epoxy group of epoxidized soybean oil

eq Equilibrium

ext External conditions

FA Formic acid

f Final value

H⁺ Protons from formic acid

HP Hydrogen peroxide

h Hydraulic (diameter)

I₂ Iodine molecule

i Index for the components

j Index for the phases

max Maximum value

O Oxygen atom

org Organic phase

PFA Performic acid

q Index for the reaction

RR Value referring to Raschig rings

r Reference value

SMX Value referring to the Sulzer SMXTM static mixer

seg Value referring to a segment of the reactor

t Value referring to the pipe

W Water

wall Wall conditions

z Value referring to the axial position

0 Feed value

Index for the Sauter mean diameter

REFERENCES

- Metzger, J. O.; Biermann, U. Sustainable Development and Renewable Feedstocks for Chemical Industry. In *ACS Symposium Series*; American Chemical Society, 2006; Vol. 921, pp 13–26. https://doi.org/10.1021/bk-2006-0921.ch002.
- (2) Barcena, H.; Tuachi, A.; Zhang, Y. Teaching Green Chemistry with Epoxidized Soybean Oil. *J. Chem. Educ.* **2017**, *94* (9), 1314–1318. https://doi.org/10.1021/acs.jchemed.6b00672.
- (3) Benecke, H. P.; Vijayendran, B. R.; Elhard, J. D. Plasticizers Derived from Vegetable Oils. US6797753B2, September 28, 2004.
- (4) De Quadros Jr., J. V.; De Carvalho, J. A. Plasticized PVC Composition. US8623947B2,

- January 7, 2014.
- (5) Corma Canos, A.; Iborra, S.; Velty, A. Chemical Routes for the Transformation of Biomass into Chemicals. *Chem. Rev.* 2007, 107 (6), 2411–2502. https://doi.org/10.1021/cr050989d.
- (6) Campanella, A.; Baltanás, M. A. Degradation of the Oxirane Ring of Epoxidized Vegetable Oils in Liquid-Liquid Systems: I. Hydrolysis and Attack by H2O2. *Lat. Am. Appl. Res.* **2005**, *35* (3), 205–210.
- (7) Campanella, A.; Baltanás, M. A. Degradation of the Oxirane Ring of Epoxidized Vegetable Oils in Liquid-Liquid Heterogeneous Reaction Systems. *Chem. Eng. J.* 2006, 118 (3), 141–152. https://doi.org/10.1016/j.cej.2006.01.010.
- (8) Campanella, A.; Baltanás, M. A. Degradation of the Oxirane Ring of Epoxidized Vegetable Oils with Hydrogen Peroxide Using an Ion Exchange Resin. *Catal. Today* 2005, 107–108, 208–214. https://doi.org/10.1016/j.cattod.2005.07.092.
- (9) Campanella, A.; Baltanás, M. A. Degradation of the Oxirane Ring of Epoxidized Vegetable Oils in Liquid-Liquid Systems: II. Reactivity with Solvated Acetic and Peracetic Acids. *Lat. Am. Appl. Res.* **2005**, *35*, 211–216.
- (10) Santacesaria, E.; Russo, V.; Tesser, R.; Turco, R.; Di Serio, M. Kinetics of Performic Acid Synthesis and Decomposition. *Ind. Eng. Chem. Res.* **2017**, *56* (45), 12940–12952. https://doi.org/10.1021/acs.iecr.7b00593.
- Olivieri, G. V.; de Quadros, J. V.; Giudici, R. Epoxidation Reaction of Soybean Oil:
 Experimental Study and Comprehensive Kinetic Modeling. *Ind. Eng. Chem. Res.* 2020, 59 (42), 18808–18823. https://doi.org/10.1021/acs.iecr.0c03847.
- (12) Santacesaria, E.; Renken, A.; Russo, V.; Turco, R.; Tesser, R.; Di Serio, M. Biphasic

- Model Describing Soybean Oil Epoxidation with H 2O 2 in Continuous Reactors. *Ind. Eng. Chem. Res.* **2012**, *51* (26), 8760–8767. https://doi.org/10.1021/ie2016174.
- (13) He, W.; Fang, Z.; Ji, D.; Chen, K.; Wan, Z.; Li, X.; Gan, H.; Tang, S.; Zhang, K.; Guo, K. Epoxidation of Soybean Oil by Continuous Micro-Flow System with Continuous Separation. *Org. Process Res. Dev.* **2013**, *17* (9), 1137–1141. https://doi.org/10.1021/op400050n.
- (14) Torrente-Murciano, L.; Bishopp, S. D.; Fox, D.; Scott, J. L. Biphasic Epoxidation Reaction in the Absence of Surfactants - Integration of Reaction and Separation Steps in Microtubular Reactors. ACS Sustain. Chem. Eng. 2016, 4 (6), 3245–3249. https://doi.org/10.1021/acssuschemeng.6b00280.
- (15) Vanoye, L.; Hamami, Z. E.; Wang, J.; de Bellefon, C.; Fongarland, P.; Favre-Réguillon, A. Epoxidation of Methyl Oleate with Molecular Oxygen: Implementation of Mukaiyama Reaction in Flow. Eur. J. Lipid Sci. Technol. 2017, 119 (5), 1600281.
 https://doi.org/10.1002/ejlt.201600281.
- (16) Phimsen, S.; Yamada, H.; Tagawa, T.; Kiatkittipong, W.; Kiatkittipong, K.; Laosiripojana, N.; Assabumrungrat, S. Epoxidation of Methyl Oleate in a TiO2 Coated-Wall Capillary Microreactor. *Chem. Eng. J.* 2017, 314, 594–599.
 https://doi.org/10.1016/j.cej.2016.12.017.
- (17) Mashhadi, F.; Habibi, A.; Varmira, K. Enzymatic Production of Green Epoxides from Fatty Acids Present in Soapstock in a Microchannel Bioreactor. *Ind. Crops Prod.* 2018, 113, 324–334. https://doi.org/10.1016/j.indcrop.2018.01.052.
- (18) Cortese, B.; De Croon, M. H. J. M.; Hessel, V. High-Temperature Epoxidation of Soybean Oil in Flow-Speeding up Elemental Reactions Wanted and Unwanted. *Ind. Eng. Chem.*

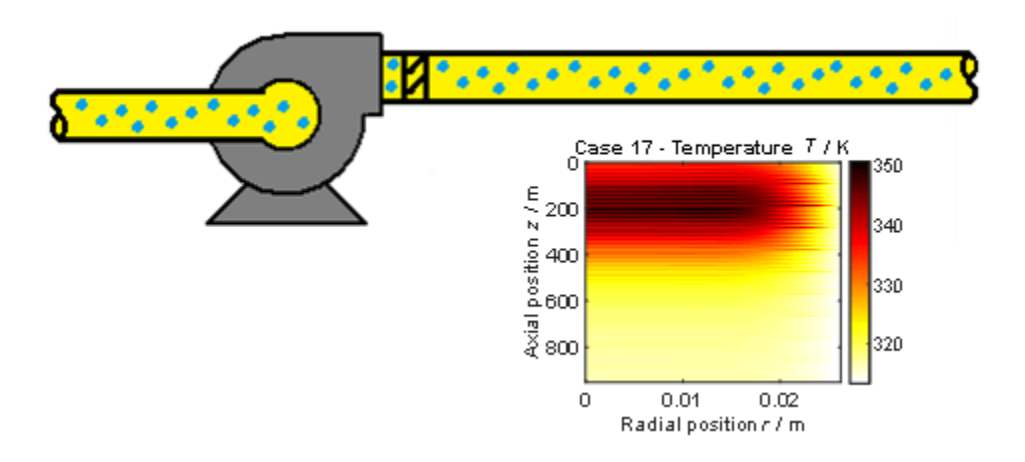
- Res. 2012, 51 (4), 1680–1689. https://doi.org/10.1021/ie200868w.
- (19) de Quadros, J. V.; Giudici, R. Epoxidation of Soybean Oil at Maximum Heat Removal and Single Addition of All Reactants. *Chem. Eng. Process. Process Intensif.* **2016**, *100*, 87–93. https://doi.org/10.1016/j.cep.2015.11.007.
- (20) Sulzer Ltd. Static mixer SMXTM plus https://www.sulzer.com/en/shared/products/static-mixer-smx-plus (accessed Sep 2, 2021).
- (21) Legrand, J.; Morançais, P.; Carnelle, G. Liquid-Liquid Dispersion in an SMX-Sulzer Static Mixer. *Chem. Eng. Res. Des.* 2001, 79 (8), 949–956.
 https://doi.org/10.1205/02638760152721497.
- (22) Bird, R. B.; Stewart, W. E.; Lightfoot, E. N. *Transport Phenomena*, 2nd ed.; John Wiley & Sons Inc.: New York, 2002.
- (23) Kim, M. H.; Kim, C. S.; Lee, H. W.; Kim, K. Temperature Dependence of Dissociation Constants for Formic Acid and 2,6-Dinitrophenol in Aqueous Solutions up to 175°C. *J. Chem. Soc. Faraday Trans.* **1996**, *92* (24), 4951–4956. https://doi.org/10.1039/FT9969204951.
- (24) Whitman, W. G. Preliminary Experimental Confirmation of the Two-Film Theory of Gas Absorption. *Chem. Met. Eng.* **1923**, *29* (3), 146.
- (25) Santacesaria, E.; Tesser, R.; Di Serio, M.; Turco, R.; Russo, V.; Verde, D. A Biphasic Model Describing Soybean Oil Epoxidation with H2O2 in a Fed-Batch Reactor. *Chem. Eng. J.* **2011**, *173* (1), 198–209. https://doi.org/10.1016/j.cej.2011.05.018.
- (26) Easton, M. F.; Mitchell, A. G.; Wynne-Jones, W. F. K. The Behaviour of Mixtures of Hydrogen Peroxide and Water: Part 1. Determination of the Densities of Mixtures of Hydrogen Peroxide and Water. *Trans. Faraday Soc.* **1952**, *48* (0), 796–801.

- https://doi.org/10.1039/TF9524800796.
- (27) Ullmann's. *Encyclopedia of Industrial Chemistry*, 7th ed.; VCH, Ed.; VCH: Weinheim, 2011.
- (28) Smith, J. M.; Van Ness, H. C.; Abbott, M. M. Introduction to Chemical Engineering Thermodynamics; McGraw-Hill, 2005.
- (29) Slawecki, T. K.; Molstad, M. C. Thermal Conductivity of Water, Glycols, and Glycol Ethers. *Ind. Eng. Chem.* **1956**, *48* (6), 1100–1103. https://doi.org/10.1021/ie50558a040.
- Ustra, M. K.; Silva, J. R. F.; Ansolin, M.; Balen, M.; Cantelli, K.; Alkimim, I. P.; Mazutti, M. A.; Voll, F. A. P.; Cabral, V. F.; Cardozo-Filho, L.; Corazza, M. L.; Vladimir Oliveira, J. Effect of Temperature and Composition on Density, Viscosity and Thermal Conductivity of Fatty Acid Methyl Esters from Soybean, Castor and Jatropha Curcas Oils. *J. Chem. Thermodyn.* 2013, 58, 460–466. https://doi.org/10.1016/j.jct.2012.10.007.
- (31) Wu, Z.; Fang, J.; Xie, Q.; Zheng, T.; Wu, L.; Lu, M.; Zhang, L.; Nie, Y.; Ji, J.
 Macroscopic Kinetics Modelling of Liquid–Liquid Reaction System: Epoxidation of Fatty
 Acid Methyl Esters. *Ind. Crops Prod.* 2018, 122 (May), 266–276.
 https://doi.org/10.1016/j.indcrop.2018.06.007.
- (32) Esteban, B.; Riba, J.-R.; Baquero, G.; Rius, A.; Puig, R. Temperature Dependence of Density and Viscosity of Vegetable Oils. *Biomass and Bioenergy* **2012**, *42*, 164–171. https://doi.org/10.1016/J.BIOMBIOE.2012.03.007.
- (33) Riazi, M. R.; Whitson, C. H. Estimating Diffusion Coefficients of Dense Fluids. *Ind. Eng. Chem. Res.* **2002**, *32* (12), 3081–3088. https://doi.org/10.1021/IE00024A018.
- (34) Nikitin, E. D.; Pavlov, P. A.; Popov, A. P.; Nikitina, H. E. Critical Properties of Hydrogen Peroxide Determined from Direct Measurements. *J. Chem. Thermodyn.* **1995**, *27* (9), 945–

- 952. https://doi.org/10.1006/JCHT.1995.0100.
- (35) Han, B.; Peng, D.-Y. A Group-Contribution Correlation for Predicting the Acentric Factors of Organic Compounds. *Can. J. Chem. Eng.* **1993**, *71* (2), 332–334. https://doi.org/10.1002/CJCE.5450710223.
- (36) Marrero-Morejón, J.; Pardillo-Fontdevila, E. Estimation of Pure Compound Properties Using Group-Interaction Contributions. *AIChE J.* 1999, 45 (3), 615–621. https://doi.org/10.1002/AIC.690450318.
- (37) Gunn, D. J. Axial and Radial Dispersion in Fixed Beds. *Chem. Eng. Sci.* 1987, 42 (2), 363–373. https://doi.org/10.1016/0009-2509(87)85066-2.
- (38) Khakpay, A.; Abolghasemi, H.; Salimi-Khorshidi, A. The Effects of a Surfactant on Mean Drop Size in a Mixer-Settler Extractor. *Chem. Eng. Process. Process Intensif.* 2009, 48
 (6), 1105–1111. https://doi.org/10.1016/j.cep.2009.02.003.
- (39) Graves, R. S.; Kollie, T. G.; McElroy, D. L.; Gilchrist, K. E. The Thermal Conductivity of AISI 304L Stainless Steel. *Int. J. Thermophys.* 1991, 12 (2), 409–415. https://doi.org/10.1007/BF00500761.
- (40) Rayner, M. Scales and Forces in Emulsification. In Engineering Aspects of Food
 Emulsification and Homogenization; CRC Press, 2015; pp 3–59.

 https://doi.org/10.1201/b18436.
- (41) Walstra, P. Principles of Emulsion Formation. *Chem. Eng. Sci.* 1993, 48 (2), 333–349.
 https://doi.org/10.1016/0009-2509(93)80021-H.
- (42) Zhang, J.; Xu, J.-Y. Rheological Behaviour of Oil and Water Emulsions and Their Flow Characterization in Horizontal Pipes. *Can. J. Chem. Eng.* 2016, 94 (2), 324–331. https://doi.org/10.1002/cjce.22377.

- (43) Fogler, H. S. *Elements of Chemical Reaction Engineering*, 5th ed.; Prentice Hall, Ed.; Prentice Hall: Upper Saddle River, 2016.
- (44) Kerr, J. A. Bond Dissociation Energies by Kinetic Methods. *Chem. Rev.* 1966, 66 (5),465–500. https://doi.org/10.1021/cr60243a001.
- (45) Blanksby, S. J.; Ellison, G. B. Bond Dissociation Energies of Organic Molecules. *Acc. Chem. Res.* **2003**, *36* (4), 255–263. https://doi.org/10.1021/ar020230d.
- (46) Di Serio, M.; Russo, V.; Santacesaria, E.; Tesser, R.; Turco, R.; Vitiello, R. Liquid-Liquid-Solid Model for the Epoxidation of Soybean Oil Catalyzed by Amberlyst-16. *Ind. Eng. Chem. Res.* **2017**, *56* (45), 12963–12971. https://doi.org/10.1021/acs.iecr.7b00881.
- (47) Santacesaria, E.; Tesser, R.; Serio, M. Di; Russo, V.; Turco, R. A New Simple Microchannel Device to Test Process Intensification. *Ind. Eng. Chem. Res.* **2011**, *50* (5), 2569–2575. https://doi.org/10.1021/ie1006307.



(For Table of Contents use only)